Enhancement of Bioactive Glass Biocompatibility by Deposition of Titanium Nanofibres Generated by the High Intensity Laser Induced Reverse Transfer Method (HILIRT)

by

Naghmeh Safaie

A thesis submitted to the
School of Graduate and Postdoctoral Studies in partial
fulfillment of the requirements for the degree of

Master of Applied Science in Mechanical Engineering

Faculty of Engineering and Applied Science

University of Ontario Institute of Technology
(Ontario Tech University)

Oshawa, Ontario, Canada

April 2020

THESIS EXAMINATION INFORMATION

Submitted by: **Naghmeh Safaie**

Master of Applied Science in Mechanical Engineering

Thesis title: Enhancement of Bioactive Glass Biocompatibility by Deposition of Titanium Nanofibres Generated by the High Intensity Laser Induced Reverse Transfer Method (HILIRT)

An oral defense of this thesis took place on < April 20, 2020 > in front of the following examining committee:

Examining Committee:

Chair of Examining Committee	Dr. Martin Agelin-Chaab
Research Supervisor	Dr. Amirkianoosh Kiani
Examining Committee Member	Dr. Dipal Patel
Thesis Examiner	Dr. Xianke Lin

The above committee determined that the thesis is acceptable in form and content and that a satisfactory knowledge of the field covered by the thesis was demonstrated by the candidate during an oral examination. A signed copy of the Certificate of Approval is available from the School of Graduate and Postdoctoral Studies.

ABSTRACT

A literature review was done in order to understand the structure and properties of the surface of bioactive glass and how to make this structure biocompatible with the human body. In this research, glass biocompatibility was increased using a deposition method called high intensity laser induced reverse transfer (HILIRT), and the samples were utilized as enhanced-biocompatibility bioactive glass (EBBG) with a correspondent nanofibrous titanium (NFTi) coating. HILIRT is an ultrafast laser method for improving implants for biomedical applications and provides a thin film of NFTi on the glass substrate. The proposed method in which NFTi samples with different structures are synthesized at various laser parameters such as power, frequency and pulse duration does not have any of the disadvantages of conventional methods such as etching. Physical properties, cell compatibility and adhesion of these NFTi prepared with different laser parameters before and after immersion in simulated body fluid (SBF) were compared.

Keywords: laser nanofabrication; nanofibrous biomaterials; biocompatibility; transparent materials

CO-AUTHORSHIP STATEMENT

This thesis and its papers were co-authored by my supervisor, Professor Amirkianoosh Kiani in the Faculty of Engineering and Applied Science at Ontario Tech University, Ontario, Canada. Secondly, this thesis and its included third paper were co-authored by Professor Holly Jones-Taggart of the Faculty of Health Sciences at Ontario Tech University, Ontario, Canada. The thesis's second paper was co-authored by Doctor Mohammad-Hossein Nasr-Esfahani and Mohammad-Hossein Beigi of the Royan Institute, Esfahan, Iran.

AUTHOR'S DECLARATION

I hereby declare that this thesis consists of original work which I have authored. This is a true copy of the thesis, including any required final revisions, as accepted by my examiners.

I authorize the Ontario Tech Univesrity to lend this thesis to other institutions or individuals for the purpose of scholarly research. I further authorize the Onratio Tech University to reproduce this thesis by photocopying or by other means, in total or in part, at the request of other institutions or individuals for the purpose of scholarly research. I understand that my thesis will be made electronically available to the public.

The research work in this thesis was performed in compliance with the regulations of Ontario Tech's Research Ethics Board.

Naghmeh Safaie

STATEMENT OF CONTRIBUTIONS

Part of the work described in this thesis has been published in journals and conferences as:

1. M. Beigi, **N. Safaie**, M. Esfahani, A. Kiani, Beigi M, "3D Titania Nanofibre-Like Webs Induced by Plasma Ionization: A New Direction for Bioreactivity Enhancement of Biomaterials", Scientific Reports, 9(1), 1-17.

2. **N. Safaie**, H. Jones-Taggart,A. Kiani, "High Intensity Laser Induced Reverse Transfer: Solution for Enhancement of Biocompatibility of Transparent Biomaterials", Coatings, 9(9), 2019, 586. https://doi.org/10.3390/coatings9090586

3. **N. Safaie**, A. Kiani, "Enhancement of bioactivity of glass by deposition of nanofibrous Ti using high intensity laser induced reverse transfer method'' published on vacuum journal, 2018, 92-99. https://doi.org/10.1016/j.vacuum.2018.08.035

4. **N. Safaie**, A. Kiani, "New Procedure of Biocompatibility Increment of Transparent Materials'' Proceedings of the 3rd International Conference of Theoretical and Applied Nanoscience and Nanotechnology (TANN'19) Ottawa, Canada, June, 2019.

5. **N. Safaie**, A. Kiani, "New Procedure of Biocompatibility Increment of Transparent Materials'' annual meeting and exposition, Washington, USA, April, 2019.

6. **N. Safaie**, A. Kiani, "Enhancement of Bioactivity of Glass by Deposition of Nanofibrous Ti Using High Intensity Laser Induced ReverseTransfer Method'' 20th conference on photonics in Montreal, Canada, June, 2018.

DEDICATION

I want to dedicate my thesis to my parents, my brother and my husband Farid, for their attentions, beliefs to me, and their love and their support.

ACKNOWLEDGEMENTS

The first and foremost thanks here is to my supervisor, Professor Amirkianoosh Kiani, who supported me through my academic journey and gave me the potential to work in the worst days of my life, who gave me a lot of support and tried to be very helpful in those days.

Secondly, I am very grateful to the staff, and members of Ontario Tech University who gave me the opportunity and provided the best ways for me to do my research.

Thirdly, I am very grateful to have NSERC (Natural Sciences and Engineering Research Council of Canada) funding for doing this research and trying to help people's lives in medical ways.

Lastly, I am very grateful to the SEM laboratories of university of Toronto and York university where provided me high quality SEM machines.

TABLE OF CONTENTS

LIST OF FIGURES

LIST OF ABBREVIATIONS AND SYMBOLS

HILIRT	High Intensity Laser Induced Reverse Transfer Method
NFTi	Nano Fibrous Titanium
SBF	Simulated Body Fluid
SEM	Scanning Electron Microscopy
XRD	X-Ray Diffraction
EDX	Energy Dispersive X-Ray Analysis
MTS	(3-(4,5-dimethylthiazol-2-yl)-5-(3-carboxymethoxyphenyl)-2-(4-sulfophenyl)-2H-tetrazolium)
MTT	3-(4,5-dimethylthiazol-2-**yl**)-2,5-diphenyl tetrazolium bromide
HAZ	Heated Affected Zone
ASTM	American Society for Testing and Materials

1. Chapter One: Introduction

1.1. Introduction

These days, with developments in tissue engineering, biomaterials are designed to be in contact with the body's organs [1, 2]. Biomaterials are utilized in medical devices and interact with the biological system [1]. Since they are used in connection with living tissues, they have to be biocompatible [1]. Amongst biomaterials, bioactive glass is used extensively in biomedical applications due to its quality of tissue regeneration and desirable properties such as excellent cell conductivity and bioactivity, controllable biodegradability, and high strength which makes them promising materials for tissue regeneration [3]. Bioactive glass, sometimes called bioglass, has the ability to form a hydroxyapatite (HA)-like surface layer when it interacts with bone cells or is soaked in simulated body fluid (SBF) [3]. The ability to make an HA-like layer in biomaterials is a desirable property since it increases the biocompatibility of materials, resulting in better interaction with surrounding living tissues and lower risk of rejection [4]. Although bioactive glass is one of the silicate-based glasses that has lower SiO_2 content and a higher CaO/P_2O_5 ratio compared to durable silicate glass [3, 5, 6], surface modification should be conducted to minimize toxicity and the possibility of failure. Some common methods to modify the surface of biomaterials are chemical etching, photolithography, and laser processing [7, 8, 9, 10, 11, 12]. The laser induced reverse transfer (LIRT) method is a novel laser processing technique that can be used to modify the surfaces of transparent materials such as glass and reduce failure of the glass after implanting in the body through optimizing the material's surface properties such as absorption, chemistry, roughness, and biocompatibility [13]. HILIRT can be employed to deposit the biocompatible metallic elements on the material's

surface to increase the generation of the HA-like layer and eventually increase cell conductivity and adhesion [13, 14, 15]. There are some metallic elements that are used in biomedical applications, especially in implant generation, such as Mg, Fe, Ti, and others. [14]. Each of these elements has its own properties, such as biodegradation, strength, and biocompatibility. Among them Mg, Fe, and their alloys are used in biodegradable implants [14], while Ti is the most biocompatible metallic element used in implant generation and scaffolds in the past [14, 16]. Ti also can be alloyed with other biocompatible elements such as Fe, Mn, Sn, and Si in medical and dental applications, as these possess high mechanical properties without metal retrogression [14, 16]. These Ti alloys are favoured as implants in hard tissue engineering such as artificial knee and hip joints, screws for fixation, bone plates, pacemakers, and artificial hearts [14, 15, 16, 17]. In dental applications Ti can be used for bridges, crowns, screws, and abutments, and as dental restoration wiring when alloyed with Ni and its own shape-memory effect. [14, 15, 16, 17]. Although Ti-6Al-4V is widely used in Ti alloys for biomedical applications due to its resistance to pitting and corrosion and its great tensile strength, there is a move to replace it with vanadium and aluminum-free alloys due to its toxic release in the body after time [14, 15, 16, 17].

Titanium in the form of nanostructured material has even higher biocompatibility and more cell conductivity because nanostructured materials have more surface area and surface roughness, which facilitate higher surface energy and better cell adhesion [14, 15, 18, 19]. In this research, we propose a novel method for the deposition of Ti nanofibrous structures on a glass substrate using the HILIRT method at different laser parameters. In this method, high laser energy can be aimed at a very small point in a very short time without changing

bulk properties; also, the laser's intensity can be high enough to remove small particles from the surface [8, 9, 12, 20]. These particles can generate a nanofibrous path on the surface of the material and can be deposited on the provided substrate [8, 9, 12, 20]. In this study we focus on the effects of laser parameters on deposited NFTi and the eventual effects of these parameters on the formation of an HA-like layer and cell adhesion. Scanning Electron Microscopy (SEM) proved the formation of Ti nanofibres on bioactive glass. Metals Technology Testing (MTT) and Energy Dispersive Spectrometry (EDS) demonstrated cell viability assessment and cell adhesion of deposited Ti coatings on bioglass after immersion in SBF solution. In comparison with the current methods for surface modification of bioglass and transparent bio materials, our proposed HILIRT method is a less time consuming, chemical-free process. In addition, any pattern generation (or redesign in pattern) on a micro and sub-micro scale is possible.

1.2. Biomaterials

Biomaterial refers to any material and structure that is in contact with the biological system of the body [21].

1.3. Type of biomaterials

Biomaterials are reliable, safe, physiologically acceptable materials that are used to make devices for disabled parts of body to make them functional [22]. They can be made from a wide range of materials such as metals, ceramics, polymers, and composites.

1.3.1. **Polymers**

Polymers are materials made from the addition of small, repetitive units called monomers [23]. The most important advantage of using polymers in making biomaterials is their ease

of shaping and their biocompatibility in comparison with ceramics and metals. Recently, polymeric biomaterials have been used in controlled released drug delivery systems. Biopolymers are divided into absorbable and non-absorbable categories [23, 24].

1.3.2. **Composites**

Composites are macroscopic compositions of two or more materials with different properties and a defined mutual surface [25]. Since a composite is the accumulation of materials with different properties, it can be suitable for biomaterials manufacturing. A good example of a biocomposite in the human body is bone structure, which includes a low-modulus background with high-modulus fibre minerals as a reinforcing material [24, 25].

1.3.3. **Metallics**

Metals are materials that can be polished and turned into various forms [24, 26]. High electrical conductivity, and high mechanical properties of metals can be their most prominent features in medicine. One of the important characteristics of metallic materials is their microstructure and the process of synthesizing, which determines the microstructure. Today, hundreds of types of metals are used as biomaterials, but in general, these metals are divided into several categories: stainless steel alloys, Co-Cr alloys, Ti and its alloys, and precious alloys [24, 26].

1.3.3.1. **Titanium and its alloys**

Titanium, a lightweight metal with a density of 4.5 g/cm^3, is very suitable for implant delivery applications. The most applicable of its alloys is an alloy of titanium with aluminum and vanadium with the name of Ti-6Al-4 [16, 17, 18, 24]. This alloy has high

tensile strength, and is a corrosion-resistant drilling alloy. Alloying elements have a great effect on the properties of titanium. For example nickel improves plasticity and adds a shape memory effect, and its alloys are used in dental orthodontics. Titanium and its alloys are covered under ASTM standards F67 [27], F136 [28] and F2063 [29] for biomedical applications [24, 29, 30].

1.3.4. **Ceramics**

Ceramics are materials that are largely non-metallic and inorganic [24, 31]. Ceramic biomaterials have properties such as high tensile strength, neutrality, and good appearance that have made them highly prestigious for implant applications [32]. Many ceramics, including nitride, carbon, and hydroxyapatite, are used for metal coatings. Bioceramics are divided into the following categories [24]:

1. Inert bioceramics,
2. Bioabsorbable ceramics,
3. Bioactive Ceramics.

1.3.4.1. **Inert Bioceramics**

Inert bioceramics have inherently low levels of reactivity in comparison with other materials such as polymers and metals in addition to resorbable ceramics [33, 34]. Examples of inert bioceramics are Al2O3 and ZrO2, which can be used in biomedical applications due to their non-toxicity [24, 33]. A major manufacturer and user of bioceramics is Japan, where there are many industries with this material, specifically in tissue engineering such as screws, ceramic drills, and plate generation [24, 34].

1.3.4.2. **Bioabsorbable Ceramics**

Bioabsorbable ceramics can degrade in the body, so there is no need for extra surgery to remove them. They are used in biomedical applications due to their mechanical properties and convenient healing procedures. The term bioabsorbable is used not only in ceramics, but also in other categories of materials such as bioabsorbable polymeric and metallic implants [35, 36].

1.3.4.3. **Bioactive Ceramics**

Bioactive glass is able to interact with biological systems and can be used in human bodies to improve tissue regeneration without any side effects. Bioactive glass maintains good contact with body organs and remains biocompatible for a long time after implementation [15, 18]. It has the potential to form a hydroxyapatite surface as a biocompatible layer after immersion in body fluid [15, 18, 37]. However, the term bioactive is not related only to the apatite basically present in the glass ceramic, but also to the apatite formation on the surface of the glass ceramic in the body. Termination of original calcium and silicate ions from the glass ceramic plays an important role in the apatite layer generation on the surface [37].

1.3.4.3.1. Bioactive glass

Bioactive glass is used extensively in biomedical applications due to its quality and effectiveness in tissue regeneration [15, 18]. Bioactive glasses are able to interact with biological systems and can be used in humans to improve tissue regeneration without any side effects. Bioactive glass is a category of glasses that maintain good contact with body organs and remain biocompatible for a long time after implementation. They have the

potential to form a hydroxyapatite surface as a biocompatible layer after immersion in body fluid [15].

1.4. Surface Modification of Biomaterials

Modification of biomaterial surfaces is a favourable way to adjust biological responses without changing material bulk properties [19]. Surface modifications are generally divided into two categories: physiochemical modification [38, 39], and surface coatings.

1.4.1. **Physiochemical Modifications**

Include chemical reactions, etching, mechanical roughening, polishing, and so forth [38, 39]. As a brief example, chemical etching is explained below.

1.4.1.1. **Chemical Etching**

This is one of the methods in which chemical materials can be diffused inside the material. This brings about a porous structure which is not desirable in implant applications [40,41,42,43]. Also, this method requires harsh chemical components and it is difficult to find each material etch [40,41,42,43]. Utilizing chemical components can cause toxic gases and unclean surfaces, which is not suitable for humans.

1.4.2. **Coating Modifications**

Surface coatings include grafting, thin film deposition, and so forth [43, 44]. As a brief example, photolithography and laser processing are explained below.

1.4.2.1. **Photolithography**

Although this method controls and handles cell behaviour and cell pattern, it needs to be done with highly extensive photomasks and is very time consuming and expensive [43, 45]

1.4.2.2. **Laser processing**

Laser processing is one of the best non-chemical methods of surface modification, in which a material's surface properties can be modified in a short period of time. This process can produce material ablation, which can result in a different surface structure, with different porosity and different chemistry without changing bulk properties for a variety of applications [15, 18, 45, 46]. In the laser procedure, emitted high laser energy is precisely directed onto a very small point in a very short time to modify the surface such as tempering up without changing the material's bulk. This is a precise and rapid method of surface modification for mass production. In addition, in this method we can change laser parameters such as laser frequency, laser intensity, etc., to get different surface structures, which makes this method very flexible for many applications [15, 18, 45, 46]. In this process the laser intensity input causes a solid's binding energy to be broken and consequently causes material removal. The entire energy delta, which can be transferred to internal energy delta u, raises the temperature of a solid to delta T considering solid's heat capacity Cp and mass m as shown in Equation (1) below [47, 48, 49]:

$$(1)\ \Delta E = \Delta U = MC_p\Delta T$$

Unlike conventional melting methods, laser energy brings about electron excitation with higher amounts than its limitation. This gives atoms more energy to destroy the structure and facilitates more rapid melting in transient time than conventional time-consuming melting [47, 48, 49]. When the laser is emitted onto the small point on the solid's surface, it encourages vaporization and removes atoms from the solid surface, thus helping the laser beam to go deeper into the material [49, 50, 51]. The depth of the laser into the solid surface

depends on the material's physical properties and the laser's frequency. Emitting laser electromagnetic fields causes electron ejection by discharging energy on the solid's surface; thus this transmitted energy causes the material's temperature to rise, producing ionized gas known as plasma. The plasma size increases around the laser emitted point and continues going up if the laser power meets the material's ablation threshold and removal of particles occurs. The plasma in this process contains ions, electrons, and nanoparticles which make the shape of plume, and while it becomes bigger the plume boundary becomes cooler than the core. Since the laser procedure is done in the air, we can expect many oxidized particles with lots of collisions and aggregations. Newly generated particles move toward the cooler region and bring about saturation, nucleation, and growth on the solid material in the form of agglomerated particles or nanofibres. The generation of agglomerated particles and nanoparticles depends on the ideality of the temperature and pressure in the laser process, and by changing laser parameters, different temperatures and pressures can be obtained [47, 48, 49, 50, 51].

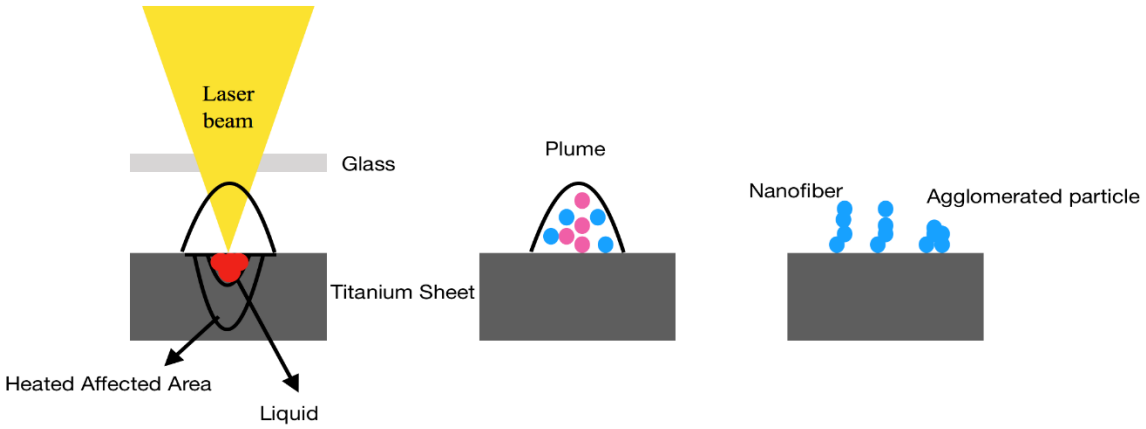

Figure 1.1: Schematic design of plume generation, and final agglomerated particles or nanofiber generation.

There are different laser machines available in the manufacturing industry such as picosecond, femtosecond and nanosecond. In femtosecond laser ablation, melting at the focal point occurs without any phase transformation, which heats up only the local point instead of bulk material, and allows better inspection of target properties. However, in picosecond and nanosecond lasers we may have a small melt region at the local point [15, 18, 19, 51].

1.5. Biocompatibility

The most important quality of a biomaterial is its ability to be in contact with human body tissues without causing any undesirable danger to that body [52, 53]. There are many different ways in which materials and tissues can mutually interact with each other. This term has been usually explained in the subject of biocompatibility [52, 53]. The word biocompatibility is extensively used within health science, but a great deal of uncertainty still exists about its actual meaning and main concept. In the past, biocompatibility was considered for items or biomaterials that should remain in the body for a long time. To be considered biocompatible, it was concluded that the biomaterials should have minimal chemical reactions with body tissues and be non-carcinogenic [52, 53]. It has further evolved that biocompatibility should relate not only to the characteristics of the biomaterial, but also to where it should be in the body [52, 53]. Biocompatibility therefore refers to the ability of a material to perform with an appropriate host response in a specific situation [53].

1.5.1. **In vitro biocompatibility**

In vitro biocompatibility tests were utilized to simulate and foresee a biomaterial's reactions with tissues when placed into the body. The in vitro analysis of biocompatibility provides less expensive ways to investigate new biomaterials; it also results in fewer animal injuries and the use of fewer laboratory materials, and it decreases the probability of trial and error while clinical methods are performed. This method of analysis is very animal friendly and is not time and money consuming [52]. Some prominent parameters of in vitro tests are explained below:

1.5.1.1. **Cell lines**

A cell line is a fixed cell culture that will proliferate without any limits indefinitely, given suitable new medium and space [19, 54]. An immortalized cell line is a population of cells from a multicellular organism which cannot proliferate in a definite pattern; however, due to mutation, the immortalized cell line avoids normal cellular senility and continues division [19, 54].

1.5.1.2. **Cell culture media**

A culture medium is a solid, liquid, or semisolid developed to aid the growth of cells or microorganisms [55]. Different types of media are used for different types of cells. Two prominent types of growth media are those used for cell culture, which use particular cell types from animals or plants, and microbiological culture, in which bacteria or fungi are grown [55].

1.5.1.3. **MTT analysis**

Life measurement, cell growth, and proliferation have different applications in research. In this enzymatic method, the reaction substrates are tetrazolium salts, and MTT is the most important of them. This simple and accurate test can evaluate the response of different cells to external factors such as growth factors, cytotoxic drugs and other chemical agents. After passage through the mitochondrial membrane, the MTT salt is affected and homogenized by the dehydrogenase 3 enzyme. The result of this homogenization process is production of purple crystals called formazan. Therefore, the more active the cell, the higher the rate of formazan 4 production, and by comparing the treatments with the control, one can become partially aware of the effects of the treatments on the metabolism of cells [19]. The MTS assay is a "one-way" MTT assay, in which the reagent is added straight to the cell culture without the intermediate steps in the MTT assay.

1.5.1.4. **Cytotoxicity**

The cytotoxicity test was the earliest in vitro test of materials and is one of the major categories of tests for the primary evaluation of materials [19, 37, 56]. It is relatively simple to design, with no need for painful animal testing. Although these days, there are some other tests for measuring the activation of biological processes, the cytotoxicity test requires fewer periods of tissue reaction to materials than others [37, 56].

1.5.1.5. **Cell adhesion**

One of the parameters of in vitro biocompatibility can be cell adhesion. Adhesion to specimens has a remarkable effect on the proliferation and differentiation of cells [19, 53]. Cell-substrate attachment is a prominent process in understanding cell shape and sustaining

cell activity and impeccability of tissues. Most of the cells have numerous functions in attaching to substrate; for example, they can be bound to an extracellular matrix or they can be attached to the other adhesive cells. The most important parts of this process are the extracellular matrix proteins, and these proteins vary in different locations in the body.

1.5.2. **In vivo biocompatibility**

In vivo biocompatibility tests were utilized to understand the exact behaviour of biomaterials with tissues when placed in the body. The in vivo analysis of biocompatibility is an expensive way to investigate new biomaterials, and it also causes animal injuries. *In vivo* "within the living" refers to trials utilizing a living organism, not a partially alive or dead organism. Animal studies and clinical experimentation are two forms of *in vivo* research. *In vivo* testing is often used over *in vitro* due to its better overall effects of watching an experiment on a living subject [57]. Although there are many reasons for believing the potential of conclusive insights about the nature of medicine or disease, there are some ways that show these conclusions can be false reasoning. For example, a therapy can be beneficial in over a short time but harmful in the long term [57].

2. Chapter Two: Experimental and theoretical methods and characterizations

2.1. Introduction

In order to evaluate the effect of different laser parameters on the titanium nanofibres produced on glass and their biocompatibility, some experimental and analytical research work was carried out. This chapter provides detailed analysis of each production method, different laser parameters, and the properties of different titanium nanofibres on the biocompatibility of specimens.

2.2. Material Synthesizing

In this research, ultrashort (picosecond and nanosecond) focused laser pulses were transmitted through transparent glass and focused on the surface of the titanium substrate. The pulse ionization process for the deposition of ablated Ti to the glass substrate was done by an Ytterbium pulsed fibre laser system at a wavelength of 1064 nm. Sample preparations were done with different powers from 6 to 12 W; a pitch of 0.025 mm; scanning speeds from 100 to 150 mm/s; frequencies from 600 to 1200 kHz; and pulse durations of 150 ps, 5 ns, and 30 ns under ambient conditions.

The specifications of the other materials, the apparatus used, and all the steps performed in this study are presented below.

2.2.1. Material specifications

2.2.1.1. Laser System

The pulse ionization process for deposition of ablated Ti to the glass substrate was performed by an Ytterbium pulsed fibre laser system (IPG Laser Model: YLPP-1-150V30) at a wavelength of 1064 nm. Figure 2.1 shows a photo of the system.

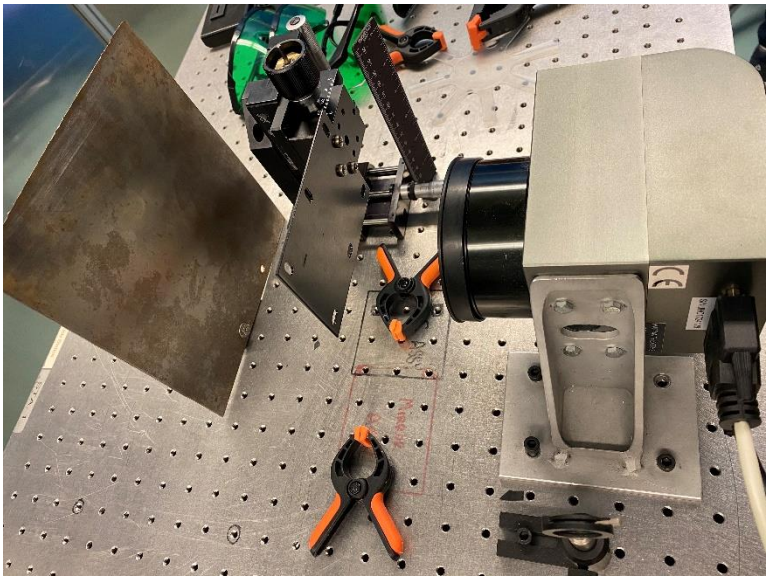

Figure 2.1: The laser system used for this project.

2.2.1.2. Titanium properties

The sheets used in this project were Grade 4 titanium, as shown in Figure 2.2.

Figure 2.2: Grade 4 Titanium sheet used in this study.

2.2.1.3. Transparent glass

The glasses utilized in this project were the biological laboratory virtual slides, as shown in Figure 2.3.

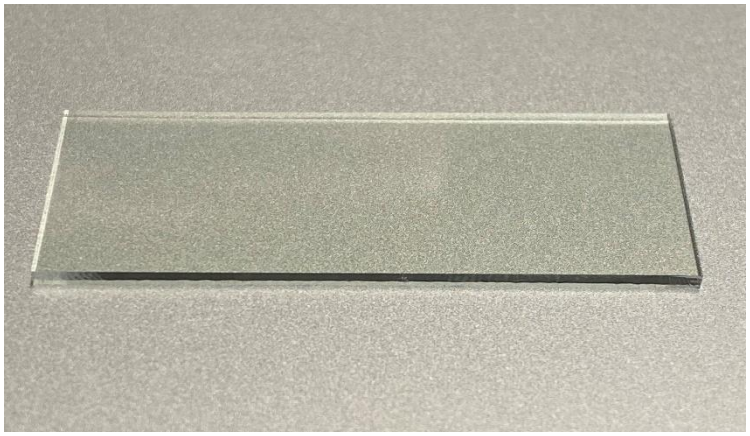

Figure 2.3: Transparent biological Laboratory virtual slides used as glass substrate.

2.2.2. Machine and system characterization

2.2.2.1. Scanning Electron Microscope (SEM)

In order to analyze Ti nanofibres deposited on bioglass and different properties of generated nanofibres such as morphology, porosity, and fibre diameter, a scanning electron microscope was used.

2.2.2.2. Energy Dispersive X-Ray (EDS)

For detecting the HA-like layer on specimens after soaking in SBF, an EDAX Genesis 4000 Energy Dispersive X-Ray (EDS) analyzer was operated.

2.2.3. Software characterization

2.2.3.1. Image Analysis

Identifying fibre diameters was done through 1.501 ImageJ software using SEM and TEM images.

2.2.3.2. X’pert software

Phase identification of XRD pattern was done with X'Pert HighScore Plus software.

2.2.3.3. MATLAB software

MATLAB R2015b software (9.6.0.1072779) was utilized for simulation of the ablation process for different ranges of laser powers and pulse repetitions.

2.2.4. Biological characterization

2.2.4.1. Simulated Body Fluid

Simulated body fluid (SBF) is a solution with similar ion concentration to human blood plasma. The SBF solution was prepared using Kokubo, T. and Takadama, H., 2006

protocol [5]. SBF is extensively used to evaluate the biocompatibility of materials via reproduction of bonelike apatite layer on the surface of artificial biomaterials and implants. In this research the laser treated samples were soaked in SBF for 3, 5, and 7 days to assess their ability to form HA-like layers.

2.2.4.2. First cell culture and biology evaluation

First cell culture studies were performed with human alveolar bone-derived mesenchymal stem cells (BMSCs) for investigation of cell-coatings' interaction and differentiation. Alveolar bone fragments obtained during orthognathic surgeries were placed over mesh covered with 4-(2-hydroxyethyl)-1-piperazineethanesulfonic acid (HEPS) medium and centrifuged at 2500 rpm to force out alveolar bone marrow cells. The cells were seeded on 25 cm^2 flasks containing alpha-modified Eagle's medium (αMEM) supplemented with 15% fetal bovine serum (FBS), L-glutamine, non-essential amino acids (NEAA) and antibiotics (penicillin 0.1 g/L; streptomycin 0.1 g/L) at 37 °C in a humidified air atmosphere containing 5% CO_2. Upon 80–90% confluency, these cells (detached with 0.05% trypsin-EDTA) were considered as passage zero (P0). P0 BMSCs were cultured and the medium was changed to fresh media every 2–3 days, at 70–80% confluency, the cells were detached using 0.25% trypsin-1 mM EDTA-4Na and seeded on NFTi coated glass and control groups at 5,000 cells per well in 48-well culture dishes. The culture medium was renewed every 3 days. (All experiments were performed using cells at passages 3–6). All chemicals and reagents, unless otherwise stated, were purchased from Sigma (St. Louis, MO). Media were purchased from Gibco, unless otherwise stated.

2.2.4.2.1. MTS Assay

An MTS assay was done in order to study the metabolic activity on NFTi coated glass as well as cell adhesion/proliferation and cytotoxicity assessments of hBMSC compared to a tissue culture plate (TCP) and uncoated glass after 4 hours and 2, 4, and 6 days of hBM-MSC seeding. In this colorimetric quantification method, cell metabolic activity is justified with a coloured formazan product which is soluble in cell culture media in a humidified atmosphere containing 5% CO2 at 37 °C, by MTS tetrazolium compound reduction. The MTS assay was treated by direct contact with NFTi coated glass with 5,000 human bone marrow-derived mesenchymal stem cells in each of 48 wells. After 4 hours and 2, 4 and 6 days after cell seeding, cells were washed with phosphate buffered saline (PBS) and incubated with a fresh medium of 20 % Cell Titer 96®Aqueous One Solution Cell Proliferation (MTS reagent) comprising serum-free medium in the dark at 37 °C in 5 % CO2 for 4 hours. Finally, aliquots were pipetted into a 96-well plate and the absorbance content of each well was figured out at 492 nm with a Fluostar Optima, BMG Lab Technologies spectrophotometric plate reader. Results were normalized as the ratio of medium without cells.

2.2.4.2.2. Immunocytochemistry

The spreading behaviour and cytoskeletal arrangement of hBMSC seeded onto the titanium coatings were studied by fluorescence microscopy using an Olympus BX61. F-actin is a family of spherical poly-operational proteins that form actin filaments which configure parts of a cell cytoskeleton. This protein, which is one of the most abundant proteins in the body, can be stained in live cells to specify and track the structure and function of cell cytoskeletons and can be seen with fluorescence microscopy. After 1 and 7 days of culture,

cells were washed with PBS and fixed with 4% formaldehyde in PBS for 15 minutes at room temperature. Then, cells were permeabilized in 1% BSA and 0.4% Triton. After washing, the permeabilizing solution, F-actin, was stained with phalloidin (actin filament, red colour, 1:300 Gibco) for 2 hours. Finally, the cell nucleus was stained with DAPI (4′,6-diamidino-2-phenylindole) (10:1000, Gibco) for 3 minutes and washed with PBS.

2.2.4.2.3. Differentiation process

Three samples of BMSC (S1, S2 and S3) were cultured on TiO2 coated glass for 21 days to induce osteogenic differentiation in comparison with a TCP and uncoated glass in an osteogenic induction medium (10 nM dexamethasone, 50 mg/ml ascorbic acid 2-phosphate, and 10 mMβ-glycerophosphate). Cells were cultured at a density of 5,000 cells per well in 48-well culture dishes in the aforementioned medium at 37 °C, 5% CO_2 for 21 days based on previous studies (19).

2.2.4.2.4. Mineralization

The ability of precipitation of inorganic materials on the organic substrate, which is called mineralization, was investigated on the samples to determine the effects of specimens on hBMSC differentiation. After 0, 7, 14, and 21 days, cells were fixed in 4% formaldehyde in PBS for 20 minutes at room temperature and stained with 0.5% alizarin red solution in water (pH= 6.4) for 2 hours. Alizarin red was dissolved in a 1M HCl solution for 2 hours with shaking. Finally, the colour intensity of each group was measured at 575 nm using potent mineralization alizarin red-positive nodules area and calcium colorimetry-based assays with a Fluostar Optima, BMG Lab Technologies spectrophotometric plate reader.

2.2.4.2.5. Gene expression analysis

Gene expression analysis is one of the tools used after days of cell seeding. Gene expression level in the bone differentiation process was measured using reverse transcriptase-polymerase chain reaction (RT-PCR) on culture on days 0, 7, 14 and 21. Total RNA was isolated with TRIZOL reagent (Invitrogen) and an RNAeasy Mini kit (Qiagen) following the manufacturer's protocol. Total RNA was pretreated with DNase I (Fermentas). cDNA synthesis was carried out with 1 μg of total RNA using random hexamer primer and the RevertAid™ H Minus First Strand cDNA Synthesis Kit (Fermentas). Real-time PCR was performed using SyBr master mix (TaKaRa) at final volume of 20-μl in a Corbett real-time PCR system (Rotor-gene 6000, Australia). The specific primers (collagen type I, osteopontin and osteocalcin) were designed with Oligo designer software version 5.2. All samples were assayed in triplicate and three independent experiments were performed. The analysis of gene expressions was performed by the ΔΔCT method, and the beta actin housekeeping gene was used to normalize the data.

2.2.4.2.6. Degradation: Ion release concentration and cell culture medium pH

One of the methods of analyzing the degradation rate of specimens in a body is by measuring the concentration of ions after days of soaking in simulated culture body media. Soaking or immersion tests can be carried out statically or dynamically. For this research, the ion release test was conducted for 1, 3, 7, 14, and 21 days via immersion of NFTi coated samples in a cell culture medium in static condition without any laminar flowing force; the ion concentration in the cell culture medium was measured after sample removal using the analytical inductively coupled plasma mass spectrometry method. In addition, the cell

culture medium pH was measured with the 827pHlab Metrohm meter after the samples were removed.

Figure 2.4: Incubator used for simulating living body conditions.

2.2.4.2.7. Protein adsorption and biocomplex adsorption/absorption

The protein adsorption of osteogenic differentiation medium for all of the surfaces without cell (A') was measured by Nanodrop at 528nm [19]. At the beginning, the light absorbance of an osteogenic differentiation specific medium was measured by Nanodrop, and the calculated amount was considered to be 100% [19]. The medium was incubated in contact with the coated, uncoated, and TCP samples at 37 ºC for 6 hours. The medium protein concentration (A) was then measured by light absorbance.

Adsorbed protein (A') (%) = 100 – A (%)

To calculate the amount of proteins which form a biocomplex with soluble ions, the medium that was in contact with the samples was centrifuged at 14000 rpm for 30 minutes (ref). This leads to biocomplex precipitation (B'). The supernatant protein concentration was measured by Nanodrop (B)

Biocomplex protein (B') (%) = A – B

To estimate the biocomplex absorption by the cells, the BMSCs was first cultured on the TiO2 coated, uncoated, and TCP samples with the osteogenic differentiation specific medium and then incubated in 37 ºC for 6 hours. Then the medium protein concentration was measured by nano drop (C). Based on the following equation, the percentage of biocomplex uptake by the cells (C') can be measured:

Biocomplex uptake by the cells (C') = (100 – A') – C

And

Adsorbed biocomplex = B' – C' (data was not shown)

2.2.4.2.8. Contact angle

The contact angle (CA), where a liquid-vapour interface meets a solid surface, describes the ability of a liquid to be in contact with a solid surface (wetting) through Young equations. In this experiment, the CA tests for cell attachment potential of specimens were performed utilizing 5 ml of distilled water droplets dropped from a distance of 1 cm and recorded 5 seconds after contact with the fabric surface using a self-developed goniometer apparatus with a high-resolution camera. The average value of three replicates measured on both sides of the drops was reported as the CA of each sample.

2.2.4.3. Second cell culture and biology evaluation

Second cell culture studies were done with human epithelial cells from the HT-29 cell line. The cells were seeded on samples for investigation on cell-coating interaction and adhesion. Epithelial cells from the HT-29 were incubated in Dulbecco's Modified Eagle Medium (DMEM) and centrifuged at 2500 rpm to force out HT-29 human epithelial cells. The cells were seeded on 25 cm^2 flasks containing alpha-modified Eagle's medium (αMEM) supplemented with 15% fetal bovine serum (FBS), L-glutamine, non-essential amino acids (NEAA) and antibiotics (penicillin 0.1 g/L; streptomycin 0.1 g/L) at 37 °C in a humidified air atmosphere containing 5% CO_2. Upon 80–90% confluence, these cells (detached with 0.05% trypsin-EDTA) were considered as passage zero (P0). Cells were cultured and the medium was changed to fresh media every 2–3 days, at 70–80% confluency, the cells were detached using 0.25% trypsin-1 mM EDTA-4Na and seeded on NFTi coated glass and control groups at 5,000 cells per well in 48-well culture dishes. The culture medium was renewed every 3 days. (All experiments were performed using cells at passages 3–6). All chemicals and reagents, unless otherwise stated, were purchased from Sigma (St. Louis, MO). Media were purchased from Gibco, unless otherwise stated.

2.2.4.3.1.MTT assay

In this research, a colorimetric metabolic activity (MTT) assay was done in order to indirectly study the viability of human cells on NFTi coated glass before and after immersion in SBF. The MTT assay was performed on 10,000 HT-29 cells incubated in media solution exposed to NFTi coated glass for 2, 4 and 6 days. After cell exposure to this media, cells were washed with PBS and incubated with a fresh serum-free medium containing dye compound 3-(4,5-dimethylthiazol-2-yl)-2,5-diphenyltetrazolium bromide

(MTT reagent) in a dark 37 ºC, 5% CO_2 humidified incubator for 4 hours. Finally, the resulting coloured solution was measured by absorbance at 500–600 nm wavelength using a multi-well spectrophotometer. Results are presented as a percentage of treated cells that remained viable compared to non-treated cells (%).

2.2.4.3.2.Cell Adhesion

Adhesion to specimens has a remarkable effect on the proliferation and differentiation of cells. To investigate cell adhesion on synthesized NFTi coatings, 104 human epithelial cells from the HT-29 cell line were seeded on samples that were sterilized with 70% alcohol in cell cultures and incubated with 5% CO2 in 37 ºC for 72 h. After incubation, the samples were washed with PBS to remove non-adherent and dead cells. Samples with adherent cells were fixed with 2.5 vol.% fixative glutaraldehyde solutions and incubated for 1 hour. The specimens were washed twice with PBS to remove the glutaraldehyde that remained, and subsequently samples were rinsed with 30%, 50%, 70%, 90% and 100% absolute ethanol for 15 minutes and taken to the SEM lab for further investigation.

2.2.4.3.3. Ccell culture medium pH and colour

For this research, the PH and colour test was conducted for 1, 3, 5 and 7 days via immersion of NFTi coated samples in a cell culture medium in static condition without any laminar flowing force; the PH in the cell culture medium was measured after solution removal from the medium with immersed samples with 827pHlab Metrohm meter.

2.3. Theoretical method

The simulation of the ablation process for different ranges of laser powers and pulse repetitions (two main laser parameters) was conducted using an analytical model in MATLAB R2015b software (9.6.0.1072779). In this research, the variable ranges of frequency and power were chosen according to the laser system functionality, from 600 to 1200 kHz and from 5 to 12 W, respectively. In the theoretical model, the 3D radial temperature gradient can be estimated by Equation (1), in which titanium diffusivity is shown as *k*; where *r* and *z* are the radius of laser spot and the depth of the laser heat affected zone respectively, and *K* is titanium thermal conductivity [58].

$$\Delta T(r,z,\tau) = \frac{I_{\max}\gamma\sqrt{k}}{\sqrt{\pi}K}\int_0^{\tau}\frac{p(\tau-t)}{\sqrt{t}\left[1+\frac{8kt}{W^2}\right]}e^{-\left[\frac{z^2}{4kt}+\frac{r^2}{4kt+0.5W^2}\right]} \quad (1)$$

Here, I_{max} is the peak intensity, and W is the beam's (1/e) field radius. Also, p(t) is related to the pulse shape and we assume we have square-shaped pulses. Additionally, the ablation depth, h(r), as a function of a radial position from the centre of the focused laser beam spot, can be anticipated by Equation (2) [58]

$$h(r) = \sqrt{-4\beta k\tau\ln\left\{\frac{\beta K\Delta T_B}{\gamma I_{\max}}\sqrt{\frac{\pi}{k\beta\tau}}\left(1+\frac{8\beta k\tau}{W^2}\right)\right\}} - \frac{r^2}{1+\frac{W^2}{8\beta kt}} \le h(0) \quad (2)$$

In Equation (2), ΔTB is equal to Tboiling − Troom temperature and β has the constant value of 0.5 for considered pulse duration, R is titanium Fresnel energy reflectivity, γ is a fraction of pulse energy absorbed by titanium, and W is the beam's field radius.

3. Chapter Three: Effect of laser power on titanium nanofibres produced on glass

3.1. Introduction

In this chapter and the following ones the effects of laser power and other parameters on produced titanium nanofibres were investigated.

3.2. Experimental Results

3.2.1. Characterization on NFTi on glass

In the HILIRT method, high laser energy can be aimed at a very small point in a very short time without changing a material's bulk properties; also, the laser's intensity, which is known as laser power, can be high enough to remove small particles from the surface [15, 17, 18, 41]. These particles can generate a nanofibrous path on the surface of the material and can be deposited on the provided substrate.

3.2.1.1. Scanning electron microscopy (SEM) images of NFTi on glass substrate with different laser powers from 5 to 12 W

As illustrated in Figure 3.1., by increasing laser power from 5 to 12 W, the amount of NFTi increased. It is also clear that a laser power of 5 W is not enough laser intensity for removing particles and ablating materials, since the surface of the microscope glass that went through laser deposition with a laser power of 5 W was similar to bare glass, with only a small amount of NFTi. This means that when a laser power of 5 W was focused over a glass surface, it raised the temperature, but not high enough to produce sufficient material ablation and remove atoms and particles from the bulk surface; therefore, the Ti atoms could not be emitted from the Ti sheet, and small amounts of nanofibres could be formed via rapid cooling process (Figure 3.1.A). Also, since by increasing laser power the shape

of deposited materials changed from agglomerated to nanostructure. As shown in Figure 3.1 and as reported before [15, 41], the surface roughness in microscale has not been changed significantly.

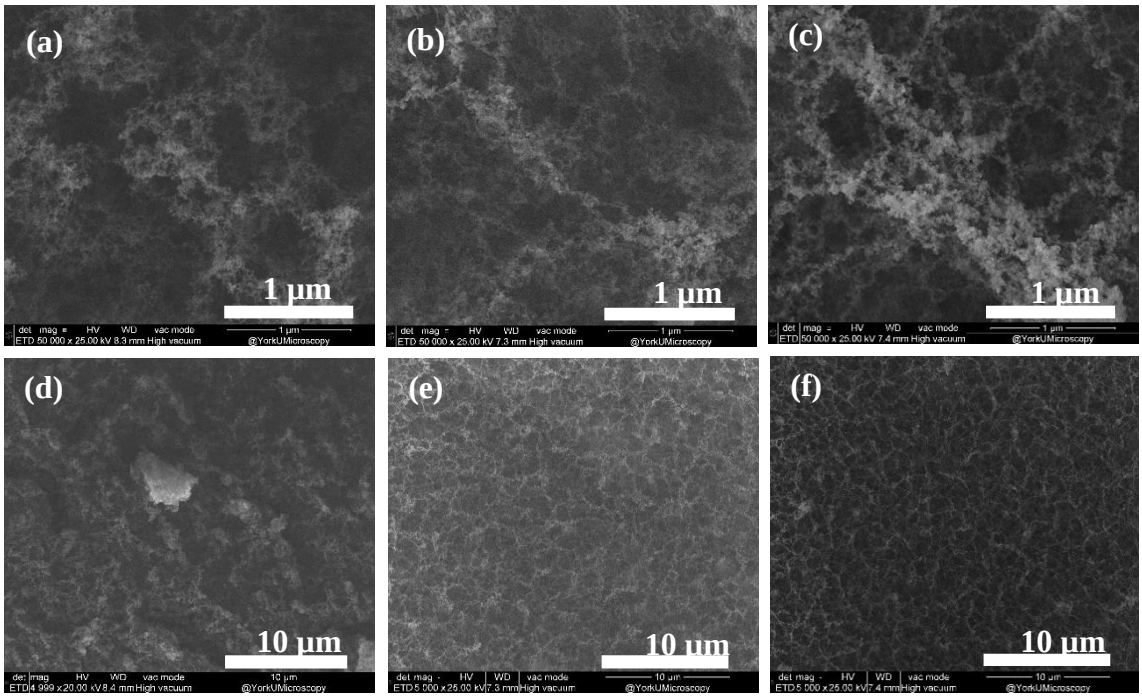

Figure 3.1: SEM images of deposited NFTi on glass substrate with (a, d) power of 5 W, (b, e) Power of 9 W, (c, f) Power of 12 W.

3.2.1.2. NFTi diameter by increasing laser power from 5 to 12 W using ImageJ and upper SEM images

By looking at the image in Figure 3.2, it is clear that the deposited titanium on the glass substrates have different diameters. By increasing laser power from 5 to 12 W the shape of the deposited titanium also changed from agglomerated nanoparticles to fibres, which means that by increasing laser power the nanofibre diameter decreased due to more fibre and fewer nanoparticles generated.

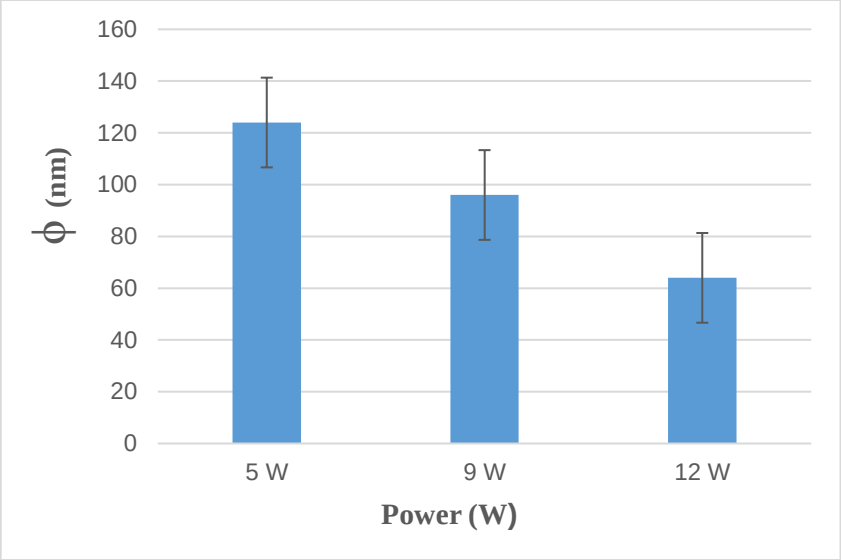

Figure 3.2: Chart of NFTi diameters by increasing laser power from 5 W to 12 W using ImageJ software.

3.2.1.3. X-Ray diffraction (XRD) of NFTi on glass substrate with different laser powers from 5 to 12 W

The XRD in Figure 3.3. shows that titanium reflected severe peaks on samples created by laser powers of 5, 9 and 12 W. It is clear from the XRD graphs that by increasing laser power from 5 to 12 W, the amount of titanium in the hexagonal close packed (hcp) also increased. Generally, increasing laser power results in injecting pulses with higher intensity on the centre of the ablation, which leads to a rise in the plume temperature and consequently more particle ablation and fibre generation.

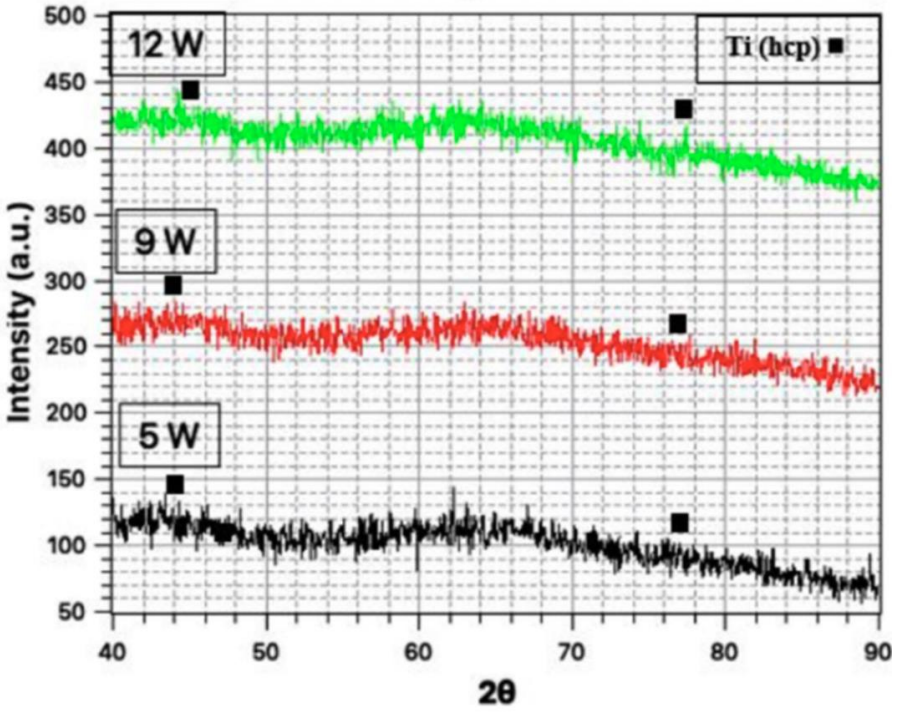

Figure 3.3: XRD pattern of NFTi on glass substrate with different laser power from 5 W to 12 W.

3.2.1.4. Raman spectrum of NFTi on glass substrate with different laser powers from 5 to 12 W

The Raman spectrum of samples produced with different laser powers shows that titanium oxide reflected severe peaks on sample 12 W in comparison with samples produced with power 5 and 9 W. It is clear that increasing laser power results in injecting pulses with higher intensity on the centre of the ablation, which leads to a rise in the plume temperature and consequently more particle ablation and fibre generation. Also, due to the fact that the samples' generation was done in a room atmosphere without any oxygen vacuum, more fibre generation leads to more titanium oxide production, which can be seen in Figure 3.4.

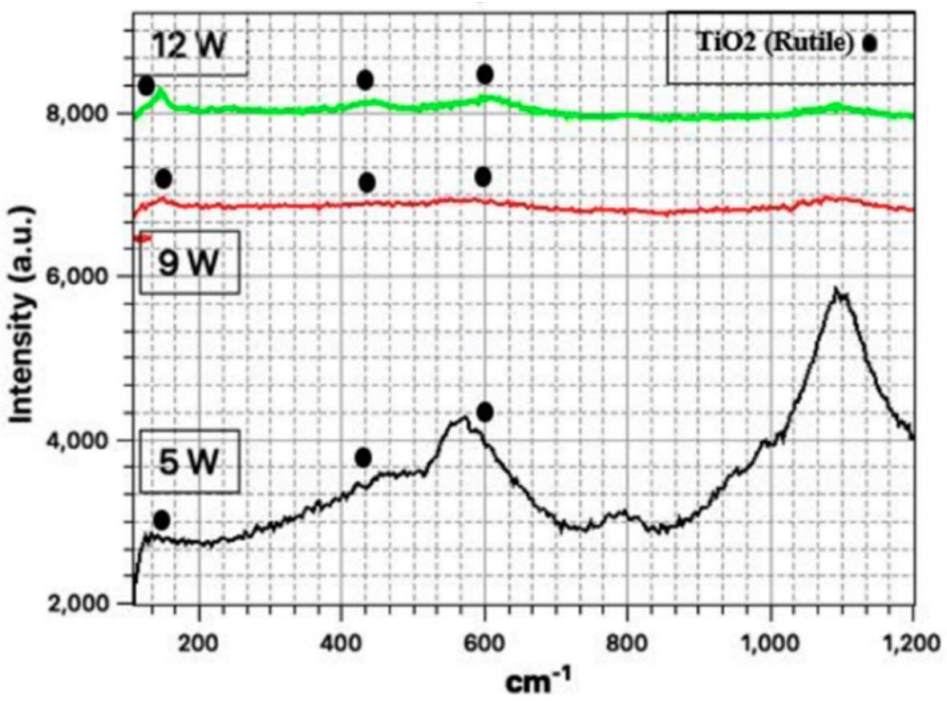

Figure 3.4: Raman spectrum of NFTi on glass substrate with different laser power from 5 W to 12 W.

3.3. Theoretical results

3.3.1. The 3D radical temperature gradient profiles by increasing laser power from 5 to 12 W

As per Equation (1) in the previous chapter, the radical temperature gradient has a direct relation to the Imax which is directly dependent on the average laser power. This means that by increasing the laser power, the temperature gradient goes up and a larger heat affected zone (HAZ) forms, as shown in Figure 3.5.

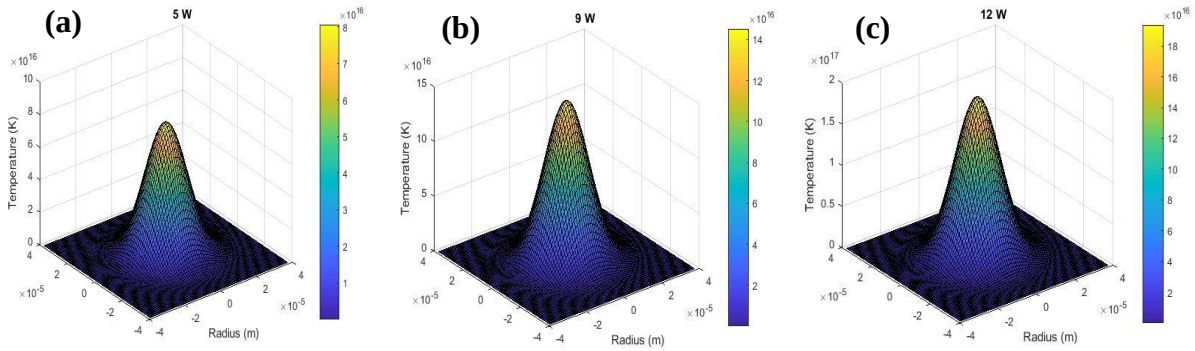

Figure 3.5: The 3D radical tempreture gradient profiles with laser power of (a) 5 W, (b) 9 W, (c) 12 W.

3.3.2. Ablation depth profiles as a function of radius and laser scanning speed for single pulsed laser by increasing laser power from 5 to 12 W

As displayed in Figure 3.6, by increasing the laser power and decreasing the scanning speed, the ablation depth increases. To further clarify, incrementing laser power while other laser parameters are constant causes the amount of the energy delivered to the Ti substrate to increase. This results in the generation of a larger HAZ and greater ablation volume on the Ti surface, which is in agreement with the results presented in Figure 3.1. The laser scanning speed has a similar behaviour, as at lower scanning speeds (higher number of pulses) more energy would be transferred to the substrate, which results in a deeper ablation profile and thicker nanofibrous layer.

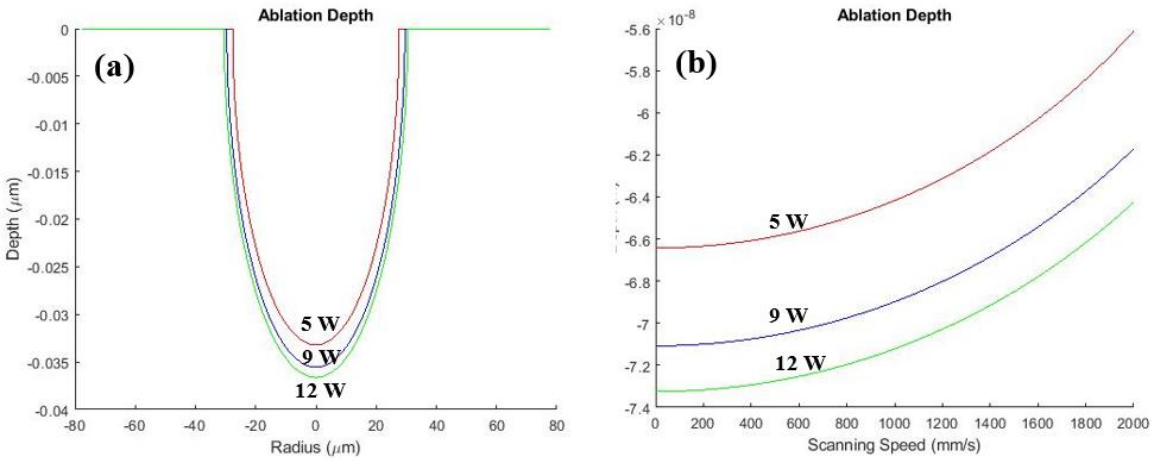

Figure 3.6: Ablation depth profiles as a function of radius. (b) Ablation depth profiles as a function of laser scanning speed for single pulsed laser by increasing laser power from 5 W to 12 W.

3.3.3. Effect of laser power on titanium nanofibres produced on glass after immersion in SBF

3.3.4. Characterization on NFTi on glass after 2 and 4 days immersion in SBF

Here, we can analyze the effect of laser power on the titanium deposited layer on glass samples after immersing them in simulated body fluid (SBF) for 2 and 4 days to simulate the body environment for samples and anticipate the samples' behaviour in body by in vitro tests.

3.3.4.1. Scanning electron microscopy (SEM) images of NFTi on glass substrate with different laser powers from 5 to 12 W after 2 and 4 days immersion in SBF

The ability to form the HA-like layer with a calcium-to-phosphorous ratio of 1.63 and other compositions of these two elements is known as biocompatibility. In order to analyze the specimens' biocompatibility, samples should be immersed in SBF. All the specimens

produced with different laser powers were immersed in SBF for 2 and 4 days, and the SEM results show the hydroxyapatite-like layer, which is a good indication of the samples' biocompatibility. Additionally, increasing laser power creates better and more consistent layers of hydroxyapatite, which can be the result of more NFTi on the samples. To illustrate further, samples with more NFTi have greater area to volume ratio of suitable places for calcium and phosphorous to nucleate and grow on, which means that they have more biocompatible surfaces, as indicated in Figures 3.7.

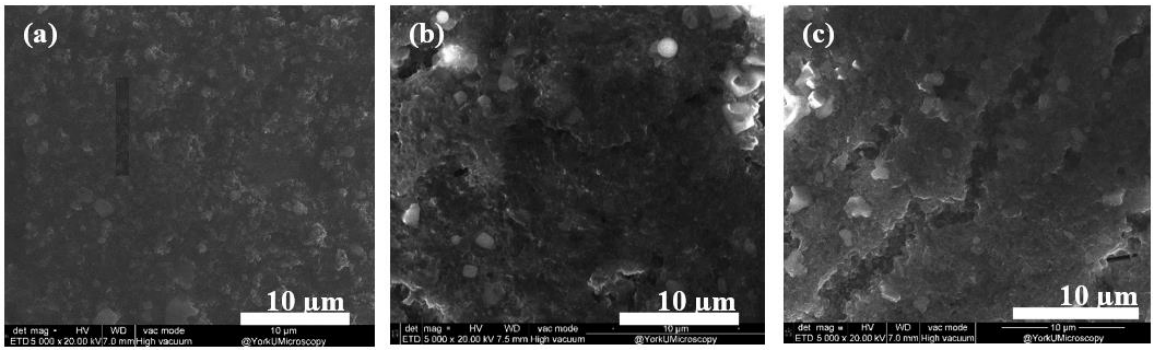

Figure 3.7: SEM images of NFTi on glass substrate with different laser power from (a) 5 W, (b) 9 W, (c) 12 W after 4 days immersion in SBF.

3.3.4.2. **X-Ray diffraction (XRD) and Raman spectrum of NFTi on glass substrate with different laser powers from 5 to 12 W after 4 days immersion in SBF**

In samples that were immersed in SBF solution for 4 days, according to the previous reported results for similar structures there are primary peaks related to HA-like composition, which can be the result of a good amount of NFTi on the samples and proper places for calcium and phosphorous to grow on, as shown in Figure 3.8. (a). The hydroxyapatite and other calcium-to-phosphorus composition peaks relating to Raman (Figure 3.8. (b)) and XRD patterns of samples which were produced by higher powers have

higher intensities compared to the samples produced by a laser power of 5 W. This can also be due to little or no generation of NFTi on the specimens produced by a laser power of 5 W, and less suitable places where calcium and phosphorous elements can start nucleating and growing [20,21].

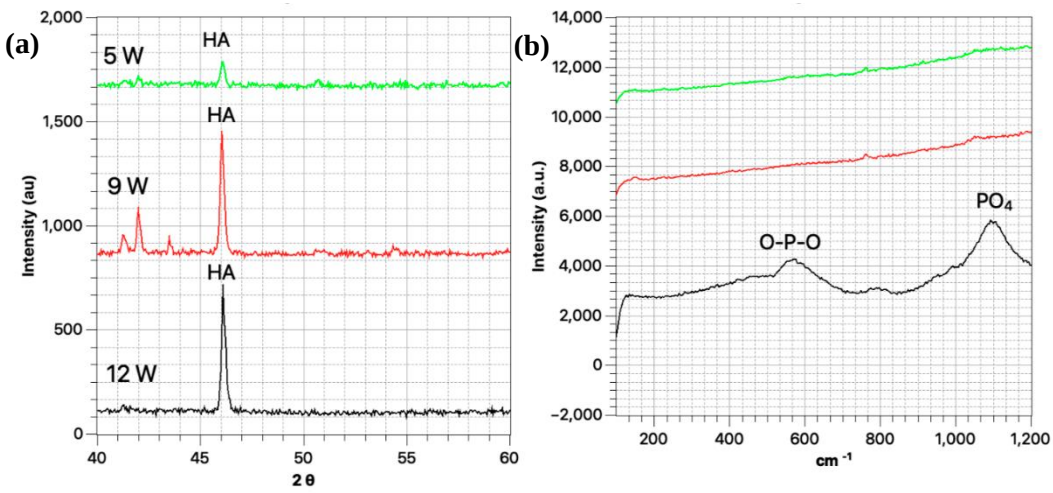

Figure 3.8: (a) XRD pattern, (b) Raman Spectrum of NFTi on glass substrate with different laser powers from 5 W to 12 W after 4 Days immersion in SBF.

3.3.4.3. **MTT results of samples produced with different laser powers before and after immersion in SBF**

Indirect MTT assay of the produced samples is shown in Figure 3.9. Generally, samples with different NFTi coatings did not show high toxicity after three days. Cell viability was constant at 100% over the period due to no toxic ion release into the test solution and no significant effect on its life properties. The solution extracted from the sample produced with a laser power of 5 W showed insignificant toxicity after immersion for 2 and 4 days in the medium. This can be representative of insufficient or less NFTi generation on the glass and no protective or compatible titanium and HA-like layers on top of the glass substrate to prevent toxic ion release, such as silicon ions, from the glass substrate [20,21].

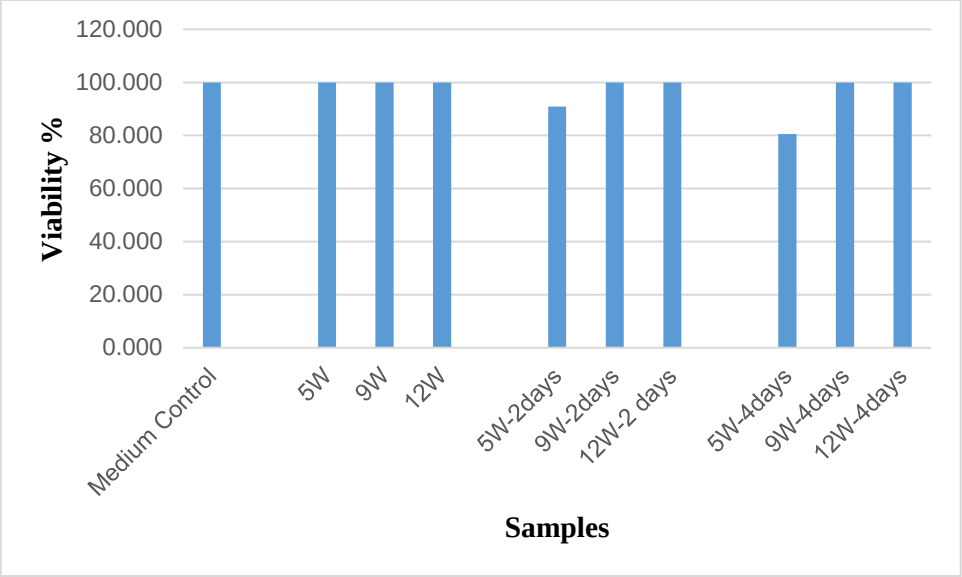

Figure 3.9: MTT results of samples produced with different laser powers before and after immersion in SBF

3.3.4.4. **SEM images of cells attached on the surface of samples produced with different laser powers**

SEM images of cell morphology and cell adhesion on samples with different laser powers are shown in Figure 3.10. Attached cells on samples produced with a laser power of 5 W can be seen in Figure 3.10. in comparison with samples synthesized with higher laser powers. Additionally, when laser power is increased, cell filopodia have more attachments on the NFTi layers, which is known as their extracellular matrix (ECM).

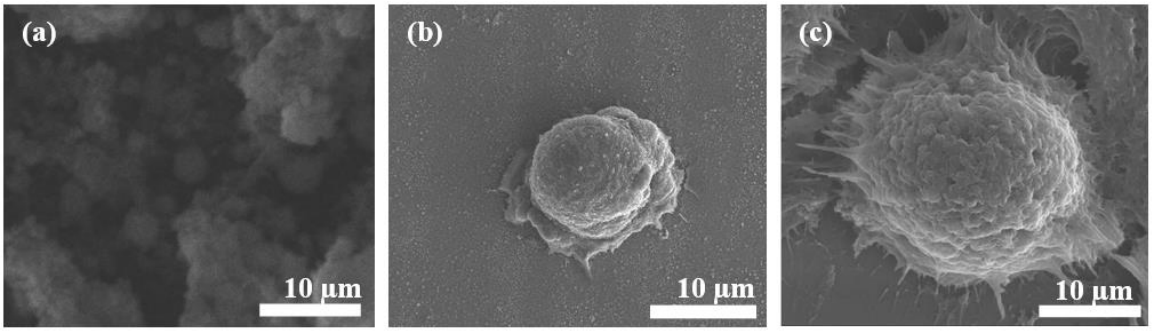

Figure 3.10: SEM images of cells attached on the surface of samples produced with laser power (a) 5 W, (b) 9 W, (c) 12 W.

3.4. Summary

Samples prepared with constant laser frequency, constant laser pulse duration and changeable laser power	Samples prepared with laser frequency = 1200 KHz, pulse duration = 150 ps, Power = 5 W	Samples prepared with laser frequency = 1200 KHz, pulse duration = 150 ps, Power = 9 W	Samples prepared with laser frequency = 1200 KHz, pulse duration = 150 ps, Power = 12 W
NFTi amount	Less	more	High
Biocompatibility	Less	more	High

4. Chapter four: Effect of laser Frequency on titanium nanofibres produced on glass

4.1. Introduction

In this chapter we describe the effect of laser frequency on produced titanium nanofibres.

4.2. Experimental Results

4.2.1. Characterization of NFTi on glass

4.2.1.1. Scanning electron microscopy (SEM) images of NFTi on glass substrate with different laser frequencies from 600 to 1200 kHz

The effect of laser frequency is shown in Figure 4.1. By increasing laser frequency from 600 to 1200 kHz, the amount of NFTi also increased. This can be due to the fact that increasing the laser frequency means decreasing pulse intervals, which leads to a shorter time between consecutive pulses and more transmitted intensity into the substrate, and therefore more heat accumulation and higher average temperature [15, 17, 18, 41]. Enhancing the spot temperature causes a denser plume and generates more ablated atoms, thus leading to more consecutive inelastic collisions, which results in the deposition of a titanium nanostructure on glass substrates [15].

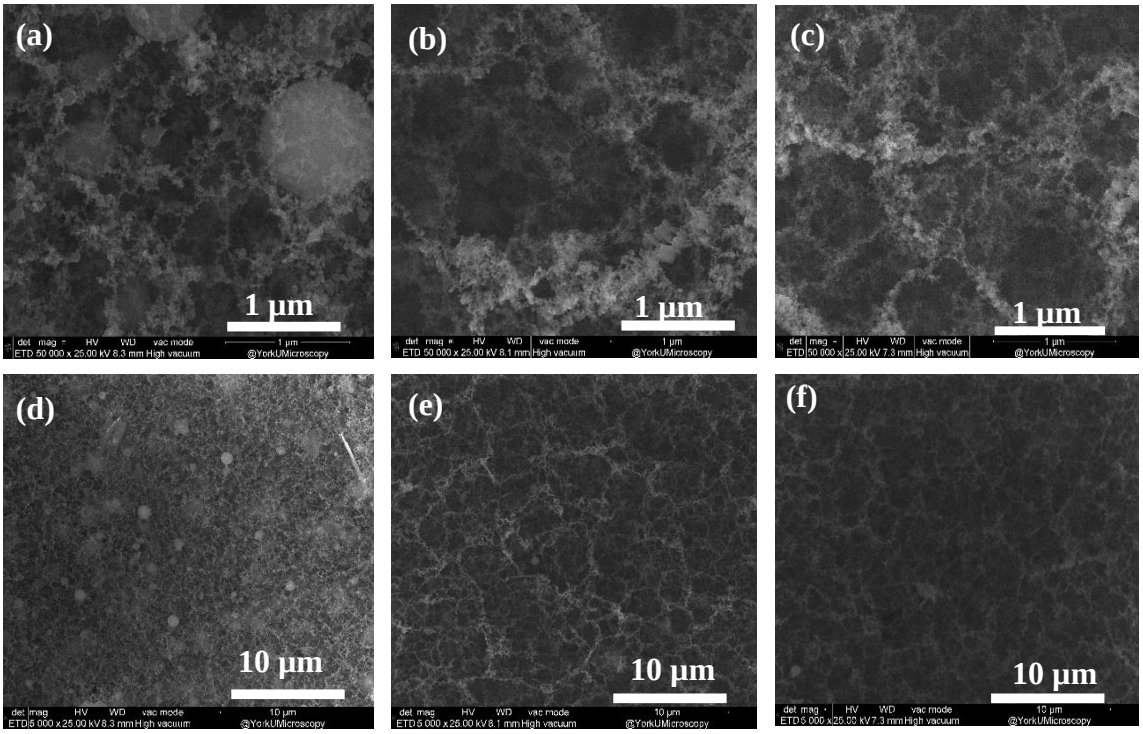

Figure 4.1: SEM images of NFTi on glass substrate with different laser frequencies of (a, d) 600 KHz, (b, e) 800 KHz, (c, f) 1200 KHz.

4.2.1.2. **Reduced NFTi diameter by increasing laser frequency from 600 to 1200 kHz using ImageJ and upper SEM images**

By increasing laser frequency from 600 to 1200 kHz, the amount of NFTi also increased. This can be due to the shorter time between consecutive pulses and more transmitted intensity into the substrate, and more ablated atoms, thus leading to more titanium nanostructure on glass substrates with shape changing from nanoparticles and agglomerated particle to nanofibres with reduced diameter [15, 18]. Figure 4.2 shows the average titanium fibre diameter deduction by enhancing laser frequency.

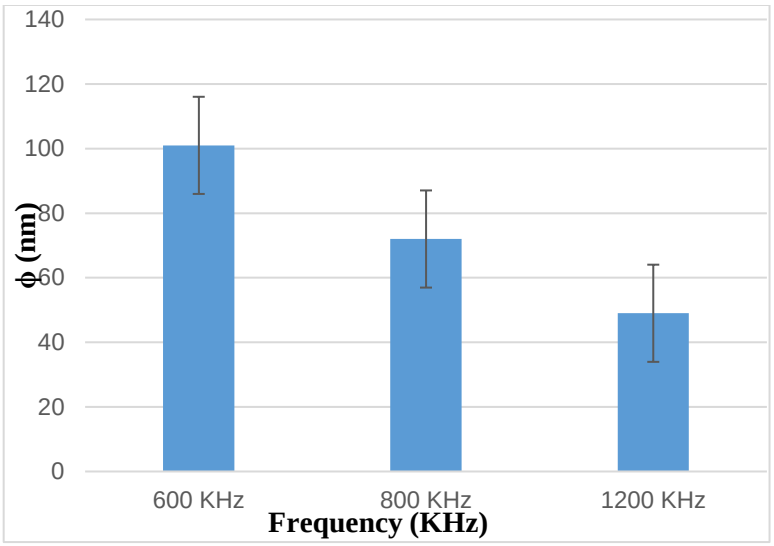

Figure 4.2: Chart of NFTi diameter by increasing laser frequency from 600 KHz to 1200 KHz using ImageJ software.

4.2.1.3. **X-Ray diffraction (XRD) of NFTi on glass substrate with different laser frequencies from 600 to 1200 kHz**

The XRD results in Figure 4.3. show severe peaks on titanium samples created by laser frequencies of 600, 800 and 1200 kHz. Generally, increasing laser frequency means a decrease in the laser pulse interval, which brings about a rise in plume temperature and consequently more particle ablations and more titanium fibre generation in the hcp phase.

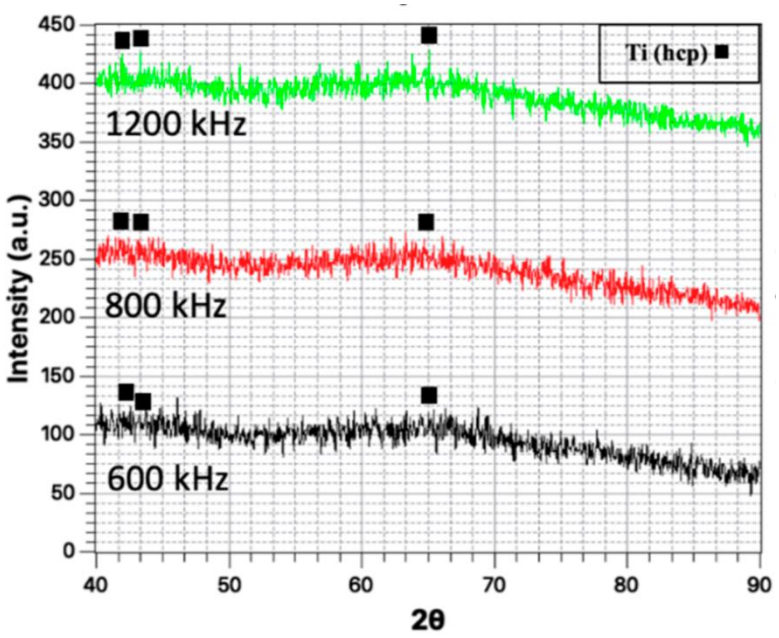

Figure 4.3: XRD pattern of NFTi on glass substrate with laser frequency from 600 KHz to 1200 KHz.

4.2.1.4. **Raman spectrum of NFTi on glass substrate with different laser frequencies from 600 to 1200 kHz**

The Raman spectrum of samples produced with different laser frequencies shows the titanium oxide peak has severe reflection on samples produced with a laser frequency of 1200 kHz compared to samples produced with frequencies of 800 and 600 kHz. It is obvious that increasing laser frequency results in shorter time between consecutive pulses and more transmitted intensity into the substrate, and more ablated titanium nanostructure on glass substrates and consequently fibre generation. Also, the condition was the same as the condition in which the laser power was changed and sample generation was done at room atmosphere without any oxygen vacuum. Performing the sample preparation in the normal room environment leads to more titanium oxide production, which is illustrated in the Raman spectrum in Figure 4.4.

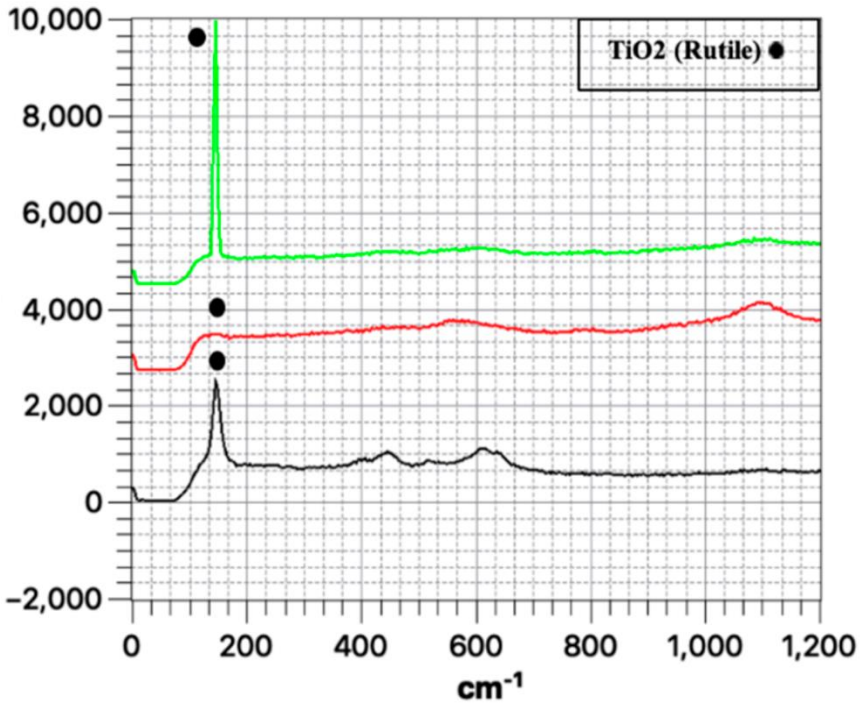

Figure 4.4: Raman spectrum of NFTi on glass substrate with different laser frequency from 600 KHz to 1200 KHz.

4.3. Theoretical results

4.3.1. The 3D radical temperature gradient profiles by increasing laser frequency from 600 to 1200 kHz

In the HILIRT method, the effect of pulse repetition needs to be considered along with the number of delivered laser pulses. Generally, at a higher pulse repetition rate and a constant average laser power, the energy of each pulse is less, which leads to a lower maximum temperature for the HAZ, as demonstrated in Figure 4.5. However, for multi-pulse processes, the average surface temperature increases by increasing the pulse repetition [15, 18, 19]. Increasing the laser repetition rate results in decreased pulse intervals (shorter time

between consecutive pulses) and a higher number of laser pulses per unit time (delivering more laser intensity into the substrate) [15-18].

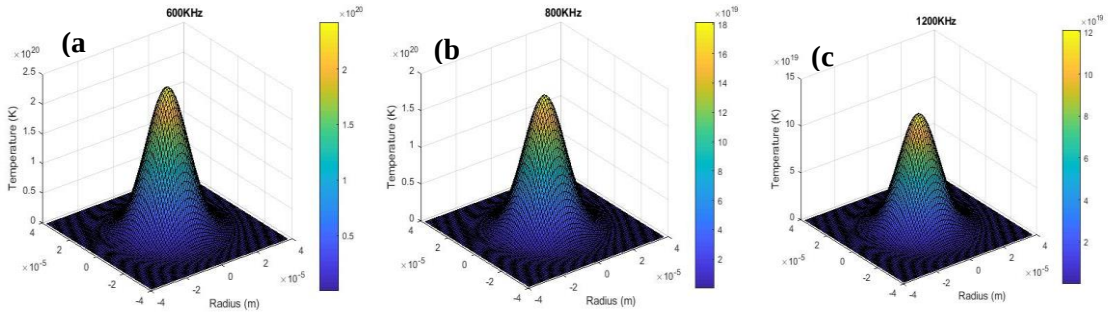

Figure 4.5: The 3D radical temperature gradient profiles for laser frequency of (a) 600 KHz, (b) 800 KHz, (c) 1200 KHz.

4.3.2. **Ablation depth profiles as a function of radius and laser scanning speed for single pulsed laser by increasing laser frequency from 600 to 1200 kHz**

As stated in the above paragraph, at higher laser repetition rates and shorter pulse intervals, denser laser plumes are formed as the average surface temperature is higher [15,18]; this causes smaller laser ablation volume and more fibres, as shown in Figures 4.5 and 4.6.

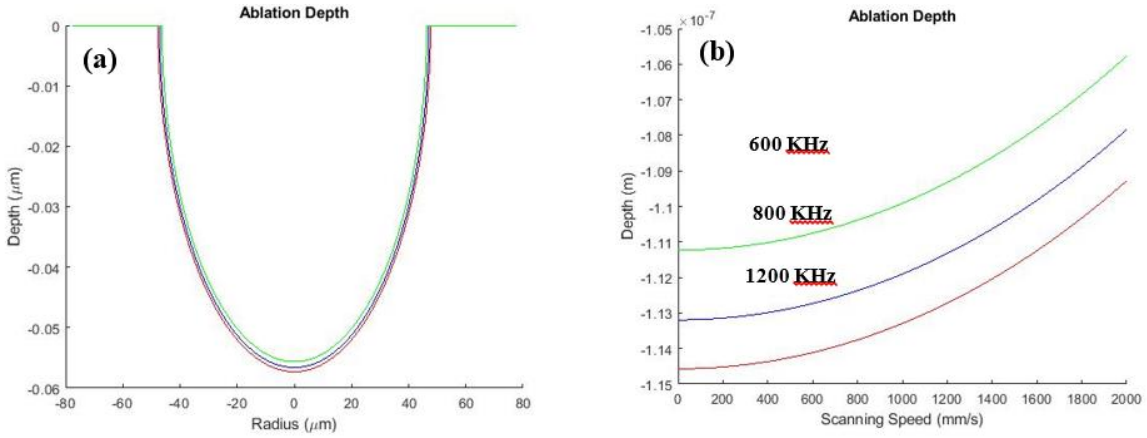

Figure 4.6: (a) Ablation depth profile as a function of radius, (b) Ablation depth profiles as a function of laser scanning speed for single pulsed laser by increasing laser frequency from 600 KHz to 1200 KHz.

4.3.3. Effect of laser frequency on titanium nanofibres produced on glass after immersion in simulated body fluid

4.3.4. Characterization on NFTi on glass after 2 and 4 days immersion in SBF

4.3.4.1. Scanning electron microscopy (SEM) images of NFTi on glass substrate with different laser frequencies from 600 to 1200 kHz after 2 and 4 days immersion in SBF

As described in the frequency parameter section above, we can analyze the effect of laser frequency on the titanium deposited layer on glass samples after putting them in SBF for 2 and 4 days to simulate the body environment and anticipate the behaviour of the samples in the body by in vitro tests.

(c)

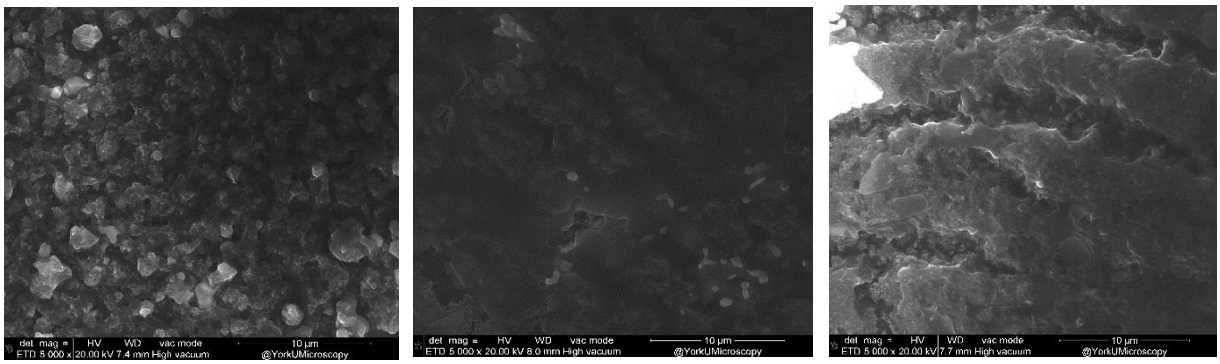

Figure 4.7: SEM images of NFTi on glass substrate with different laserr frequency from (a) 600 KHz, (b) 800 KHz, (c) 1200 KHz after 4 days immerson in SBF.

Samples produced with different laser frequencies were immersed in SBF for 2 and 4 days, and the SEM results show the HA-like layer, which is a good indication of the samples' biocompatibility. Additionally, increasing laser frequency similar as increasing laser power, creates better and more consistent layers of HA-like layer which can be the result of more NFTi on the samples. To explain more, samples with more generated NFTi have greater area to volume ratio of biocompatible areas for calcium and phosphorous to nucleate and grow on, as indicated in Figures 4.7.

4.3.4.2. X-Ray diffraction (XRD) and Raman spectrum of NFTi on glass substrate with different laser frequencies from 600 to 1200 kHz after 4 days immersion in SBF

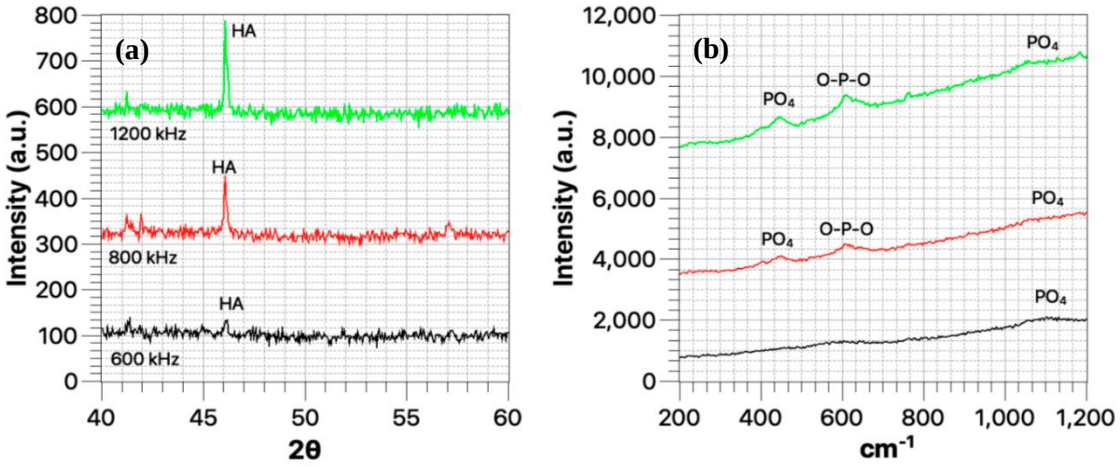

Figure 4.8. (a) XRD pattern, (b) Raman spectrum of NFTi on glass substrate with different laser frequency from 600 KHz to 1200 KHz after 4 days immersion in SBF.

In samples immersed in SBF solution there are several peaks related to HA-like layers which are the result of a good amount of NFTi on the samples and good places for calcium and phosphorous to develop. As illustrated in Figure 4.8, the hydroxyapatite and other calcium to and phosphorous to phosphorus composition peaks relating to Raman and XRD patterns of samples produced by higher laser frequencies have higher intensities compared to the sample produced by a laser frequency of 600 kHz. This can be due to little or insufficient generation of NFTi on the sample produced by the laser frequency of 600 kHz, and less desirable places for calcium and phosphorous elements to start growing. Also, similar to laser power, the sample produced with the highest laser frequency has a drastic upper shift in the Raman spectrum which can be due to the thicker NFTi coating generation.

4.3.4.3. **MTT results of samples produced with different laser frequencies before and after immersion in SBF**

Indirect MTT assay of the produced samples is shown in Figure 4.9. Generally, indirect MTT assay of the produced samples is shown in Figure 26. Generally, samples with different NFTi coatings did not show high toxicity after three days. Cell viability was constant at 100% over the period due to no toxic ion release into the test solution and no significant effect on its life properties. There is no difference between the cell viability of the different laser frequencies (almost 100% viability), and this can be indicative of a sufficient or high amount of NFTi on the glass and compatible titanium and HA-like layers on top of the glass substrate to prevent toxic ions in the medium.

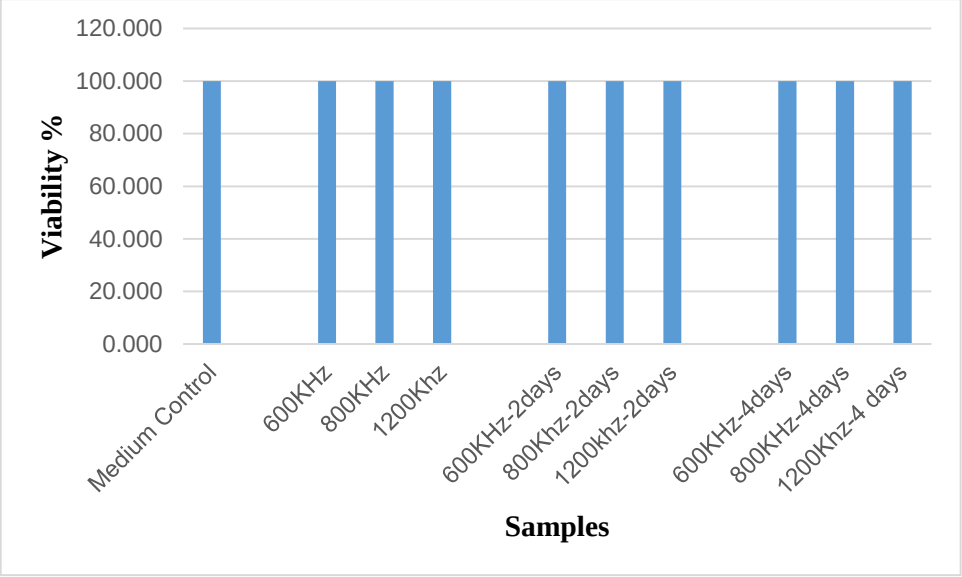

Figure 4.8: MTT results of samples produced with different laser frequency before and after 2 and 4 days immersion in SBF.

4.3.4.4. SEM images of cells attached on the surface of samples produced with different laser frequencies

SEM images of cell morphology and cell adhesion on samples with different laser powers are shown in Figure 3.10. Attached cells on samples produced with a laser frequency of 600 kHz can be seen in Figure 4.10(e), in comparison with samples synthesized with higher laser frequencies. The SEM results illustrate that cells adhered better on NFTi surface than on bare glass and they adhered better and seemed healthier at higher frequency samples. This shows the biocompatibility of NFTi on the coating produced with higher frequencies and the preference of cells to be fitted on an NFTi coating rather than bare glass (Figure 4.10(a, b)). Additionally, cell filopodia have more attachments on the NFTi layers, which is known as their extra cellular matrix (ECM), with increasing laser frequency. Cell bodies show less degradation and disappearance during the fixing process, which means that increasing laser frequency brings about more NFTi generation and thicker NFTi layers on the glass substrate, with higher surface-to-volume ratio and more compatible and available places as ECM for cell filopodia to connect and adhere to [21].

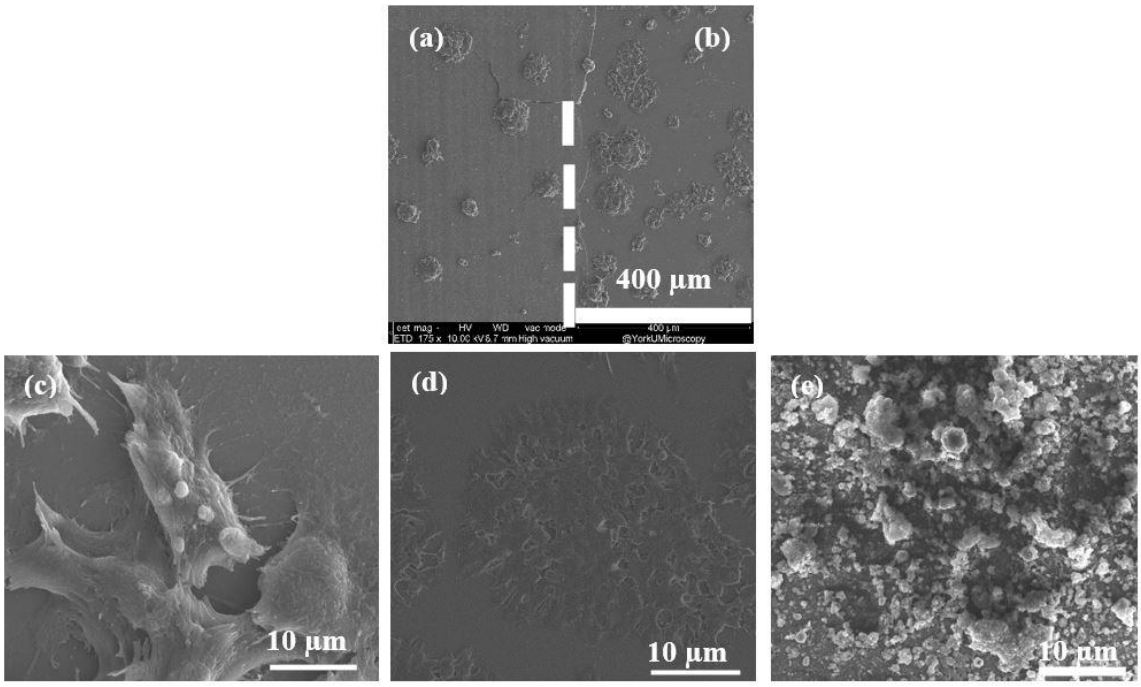

Figure 4.9: SEM images of cells attached on the surface of samples produced with (a) 800 KHz on NFTi-coated glass, (b) 800 KHz on bareglss, (c) 1200 KHz, (d) 800 KHz, (e) 600 KHz.

4.4. Summary

Samples prepared with constant laser power, constant laser pulse duration and changeable laser frequency	Samples prepared with laser power = 9 W, pulse duration = 150 ps, frequency = 600 KHz	Samples prepared with laser power = 9 W, pulse duration = 150 ps, frequency = 800 KHz	Samples prepared with laser power = 9 W, pulse duration = 150 ps, frequency = 1200 KHz
NFTi amount	Less	more	High
Biocompatibility	Less	more	High

5. Chapter five: Effect of laser power on titanium nanofibres produced on glass

5.1. Introduction

The aim of this chapter is to explain the effect of laser pulse duration on the deposited Ti structures on bioactive glass using high intensity laser induced reverse transfer (HILIRT), which is proposed as a new method for the enhancement of biocompatibility of glass and transparent materials for the deposition of Ti nanofibrous structures.

5.2. Experimental Results

Titanium nanofibres with different porosity and biocompatibility are synthesized at various pulse durations with the HILIRT method. Features and biocompatibility of these deposited Ti coatings before and after 4 days immersion in SBF were compared.

5.2.1. **Characterization of NFTi on glass substrate**

5.2.1.1. **SEM images of NFTi on glass substrate with different laser pulse durations from 150 ps to 30 ns**

By increasing laser pulse duration (τ), the ablated titanium particle structure to be deposited on the glass substrate changes from a nanofibrous structure to agglomerated structures as shown with different magnification in Figure 5.1 (a) to 5.1 (c) and 5.1 (e) to 5.1 (g). In the other words, evaporation occurs from the metal liquid, generating precise agglomerated particles of metal on the substrate, which is not ideal for nanofibre generation. The electrons of the solid target absorb laser energy, while a high temperature laser pulse interacts with that target and the electrons' energy is conducted to the lattice very rapidly. In the ultrashort pulsed laser system, energy is conducted to the substrate electrons more

quickly than the transition of energy from those electrons to the lattice of the material, and accordingly, the ultrashort process is a precise method of machining with the least thermal waste.

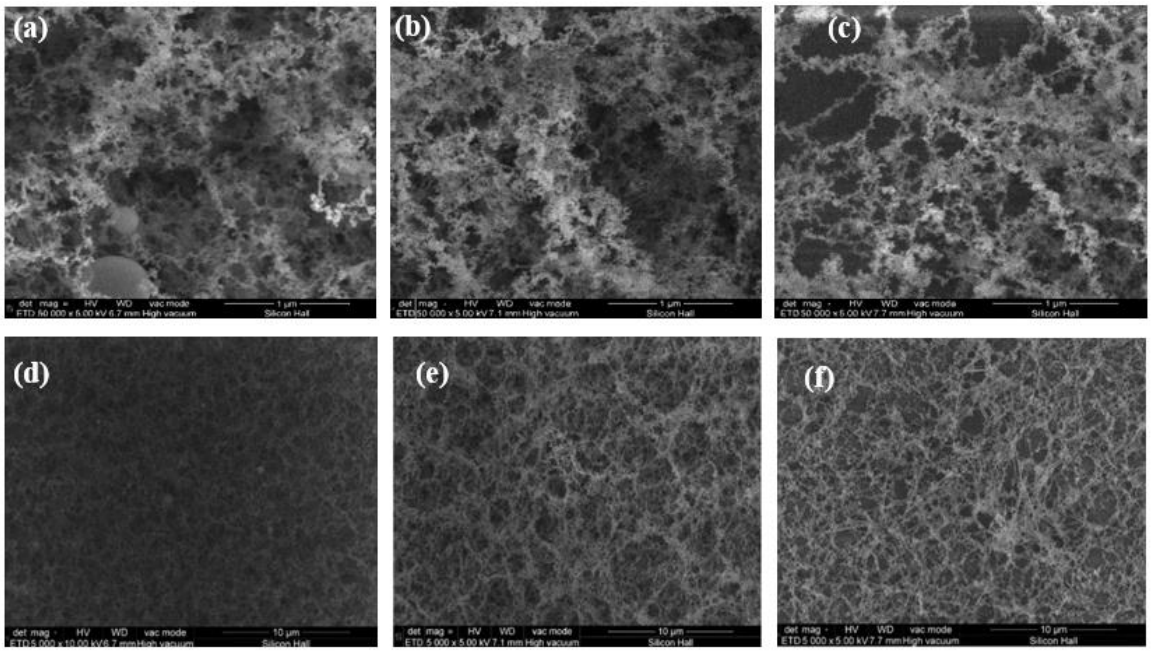

Figure 5.1: SEM images of NFTi on glass substrate produced with laser pulse duration of (a, d) 150 ps, (b, e) 5 ns, (c,f) 30 ns.

5.2.1.2. **X-Ray diffraction (XRD) of NFTi on glass substrate with different laser pulse durations from 150 ps to 30 ns**

As displayed in Figure 5.2, the titanium (alpha) and titanium oxide phases reflected very severe peaks on samples created by a laser pulse duration of 150 ps, and weak peaks on samples generated with 5 ns and 30 ns pulse durations, which is the result of less titanium generation on the samples. Decreasing pulse duration means laser radiation with more intensity and local heating, which cause local metal fragmentation. This was seen more in samples generated by 150 ps in comparison with samples generated by 30 ns.

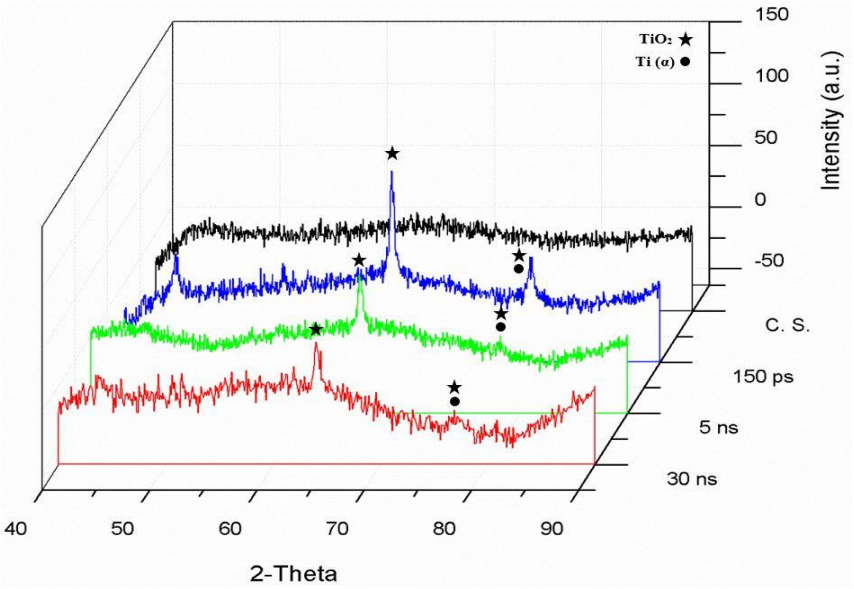

Figure 5.2: XRD pattern of NFTi on glass substrate with laser pulse duration from 150 ps to 30 ns.

5.2.1.3. **Raman spectrum of NFTi on glass substrate with different laser pulse durations from 150 ps to 30 ns**

This section describes the Raman spectrums at room temperature for analyzing the chemical composition of samples generated by different laser pulse durations.

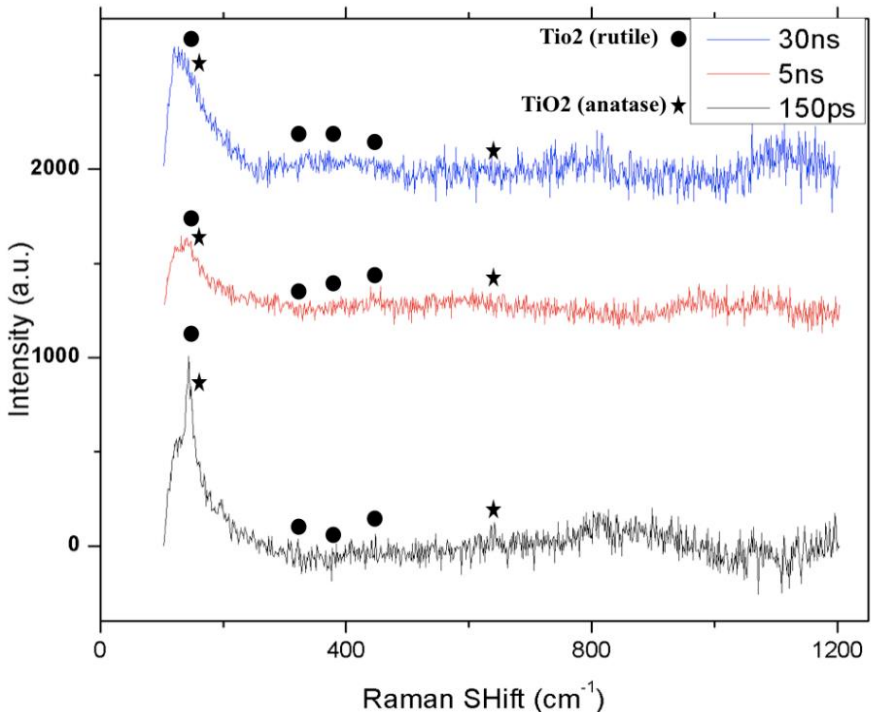

Figure 5.3: Raman spectrum of NFTi on glass substrate with different laser pulse durations from 150 ps to 30 ns.

The micro-Raman results in Figure 5.3 agree with the EDX and XRD results as peaks of both TiO2 phases (rutile and anatase) slightly increase by decreasing the pulse duration. Although the electrons of the solid target absorb laser energy, while a high temperature laser pulse interacts with that target and electrons, energy is quickly conducted to the lattice [41].

5.3. Theoretical results

5.3.1. **3D radical temperature gradient profiles for increasing laser pulse duration from 150 ps to 30 ns**

As described in Chapter 3 (Equation 1), the temperature gradient can be roughly estimated by the equation above in which r is the radius of the laser spotted area and z is the depth of the laser affected area.

In this equation p(t) can be assumed with the value of 1 for a theoretical square-shaped pulse at the centre point of the HAZ. Therefore, the temperature profile at the centre and surface of ablation can be seen in Figure 5.4 at different pulse durations; the calculated temperature profile in Figure 5.4 indicates that a shorter laser pulse duration results in deeper and higher temperatures in the HAZ [41, 60].

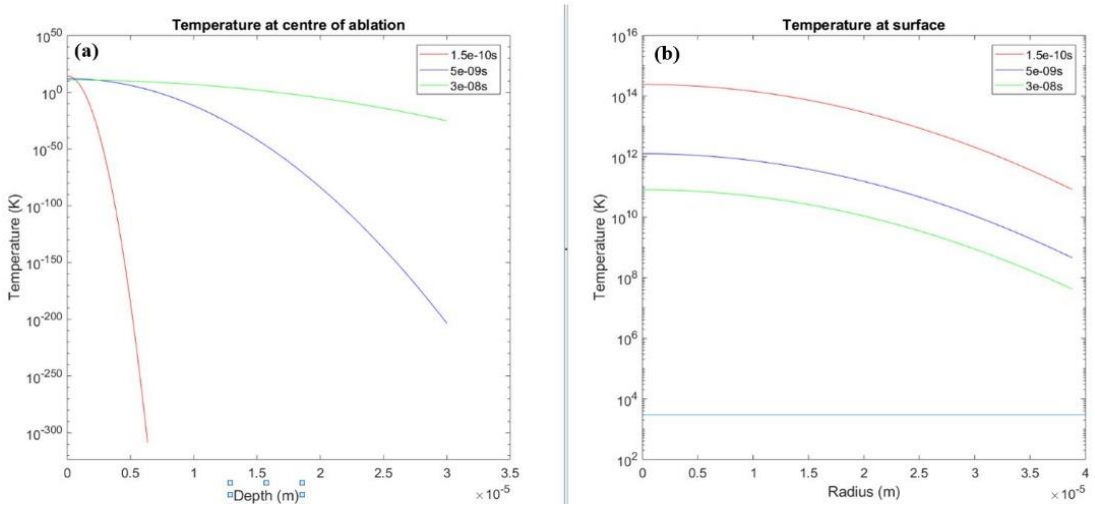

Figure 5.4: (a) Ablation depth profile as a function of radius, (b) Ablation depth profiles as a function of laser scanning speed for single pulsed laser by increasing laser pulse duration from 150 ps to 30 ns.

The temperature gradients as a function of r and z for pulse durations of 150 ps, 5 ns, and 30 ns are shown in Figure 5.5 (a) to (c). The computed results clearly show the temperature of the irradiated zone is significantly higher for the shorter pulse duration of 150 ps in comparison with 5 ns and 30 ns.

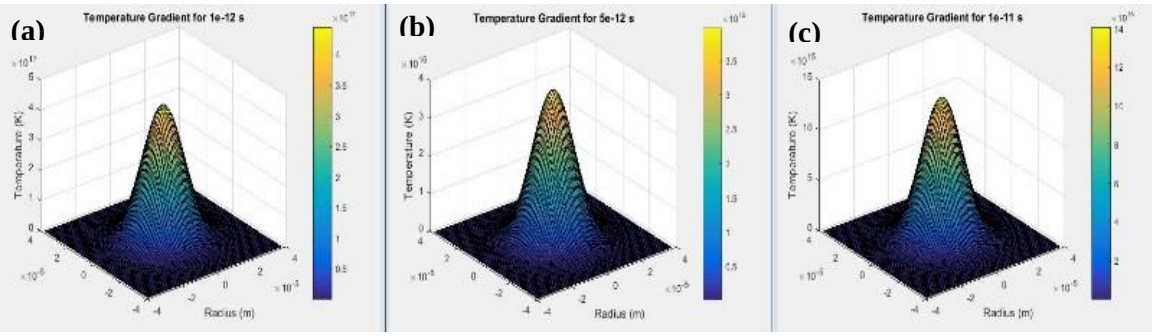

Figure 5.5: The 3D radical tempreture gradient profiles with laser pulse duration of (a) 150 ps, (b) 5 ns, (c) 30 ns

5.3.2. **Ablation depth profiles as a function of radius for single pulsed laser by increasing laser pulse duration from 150 ps to 30 ns**

The ablation depth as a function of r for 3 different pulse durations is illustrated in Figure 5.6. As shown in the graph, the ablated zone for the shortest pulse duration of 150 ps is shallower, as we have more heat accumulation and a smaller HAZ. The theoretical results presented so far are in agreement with the experimental results, as the shorter pulse duration results at higher ablation temperature lead to generation of a denser plasma plume at a higher temperature; thus, more NFTi structures were formed on the glass substrate in this process.

$$\Delta T(r,z,\tau)=\frac{I_{\max}\gamma\sqrt{\kappa}}{\sqrt{\pi}K}\int_0^{\tau}\frac{p(\tau-t)}{\sqrt{t}[1+\frac{8\kappa t}{W^2}]}e^{-[\frac{z^2}{4\kappa t}+\frac{r^2}{4\kappa t+0.5W^2}]}dt$$

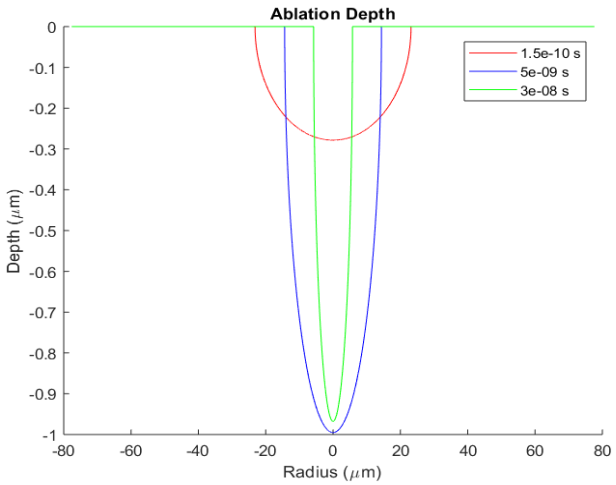

Figure 5.6: Ablation depth profiles as a function of radius for single pulsed laser by increasing laser pulse duration from 150 ps to 30 ns.

5.3.3. **Effect of laser pulse duration on titanium nanofibres produced on glass after immersion in SBF**

5.4. Characterization on NFTi on glass after 2, and 4 days immersion in SBF

5.4.1. **Scanning electron microscopy (SEM) images of NFTi on glass substrate with different laser pulse durations from 150 ps to 30 ns after 2 and 4 days immersion in SBF**

As expected, by increasing laser pulse duration, less HA and other calcium and phosphor compositions were deposited on the Ti coated samples [18]. This can be the result of less nanofibre generation on Ti coated glass substrate at a higher laser pulse duration.

Decreasing the laser pulse duration means creating more biocompatible Ti nanofibres which absorb more HA-like content on the samples as shown in Figure 5.7 (c,f) and (a,d)) [26].

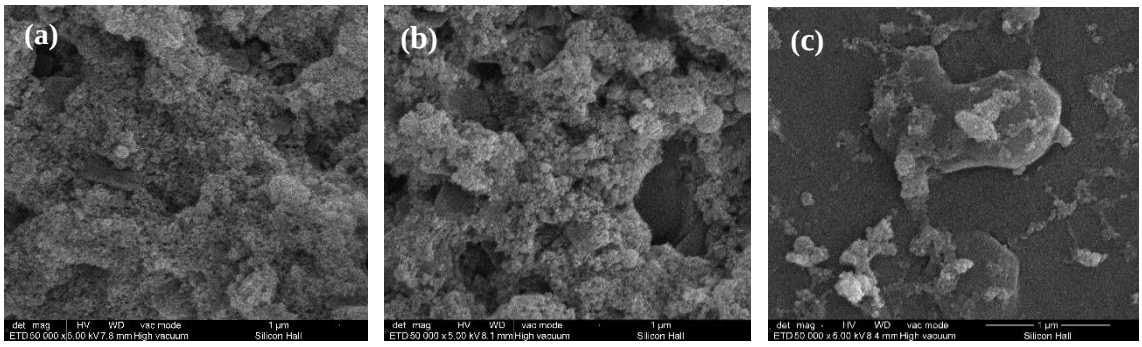

Figure 5.7: SEM images of NFTi coatings produced on glass substrate with different laser pulse duration of (a) 150 ps, (b) 5 ns, (c) 30 ns after 4 days immersion in SBF.

5.4.2. **X-Ray diffraction (XRD) and Raman spectrum of NFTi on glass substrate with different laser pulse durations from 150 ps to 30 ns after 2 and 4 days immersion in SBF**

The elevation of HA-like layer peaks in XRD patterns of the corresponding samples in Figure 5.8 (a,c) and other relevant compositions of calcium and phosphate in the Raman spectrum in Figure 5.8 (b,d) agree with the XRD results. Decreasing laser pulse duration and eventually creating more NFTi with higher SVR would provide more sites for nucleation and growth of different calcium and phosphate minerals such as hydroxyapatite, and Octa calcium phosphate (OCP) with calcium-to-phosphate weight percentage ratios of 1.67 and 1.33 respectively [60]. Consequently, more biocompatibility and less rejection after implanting in the body is possible for the samples prepared at lower pulse duration [10].

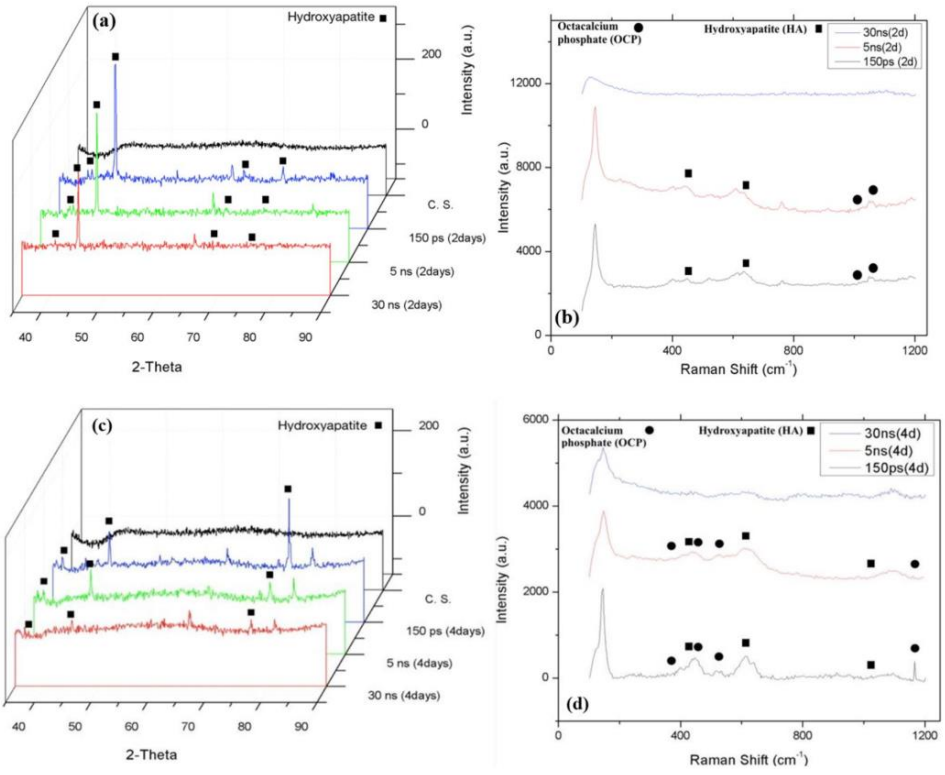

Figure 5.8: (a) XRD pattern, (b) Raman spectrum of NFTi on glass substrate with different laser pulse duration after 2 days immersion in SBF, (c) XRD pattern, (d) Raman spectrum of NFTi on glass substrate with different laser pulse duration after 2 days immersion.

5.4.3. **MTS results of samples produced with different laser pulse durations before and after immersion in SBF**

The cytotoxicity of TiO2 coatings were determined by the MTS assay of the BMSC (Figure 5.9 (a)). Four hours after cell seeding, MTS assay was used to show the amount of cell attachment on the different samples. Sample S1 had the highest OD compared to the other samples. The uncoated sample shows the lowest absorbance, the OD of the control-TCP was significantly lower than S2, and no significant difference was observed between the control-TCP and S3.

To assess the cell viability, MTS assay was used on days 2, 4, and 6. The colour absorbance quantity for all samples increased continuously with the culture time relative to the number of primary cells adhering, demonstrating a normal growth trend and worthy cytocompatibility. It is clear that all treated samples were better than the untreated glass and TCP.

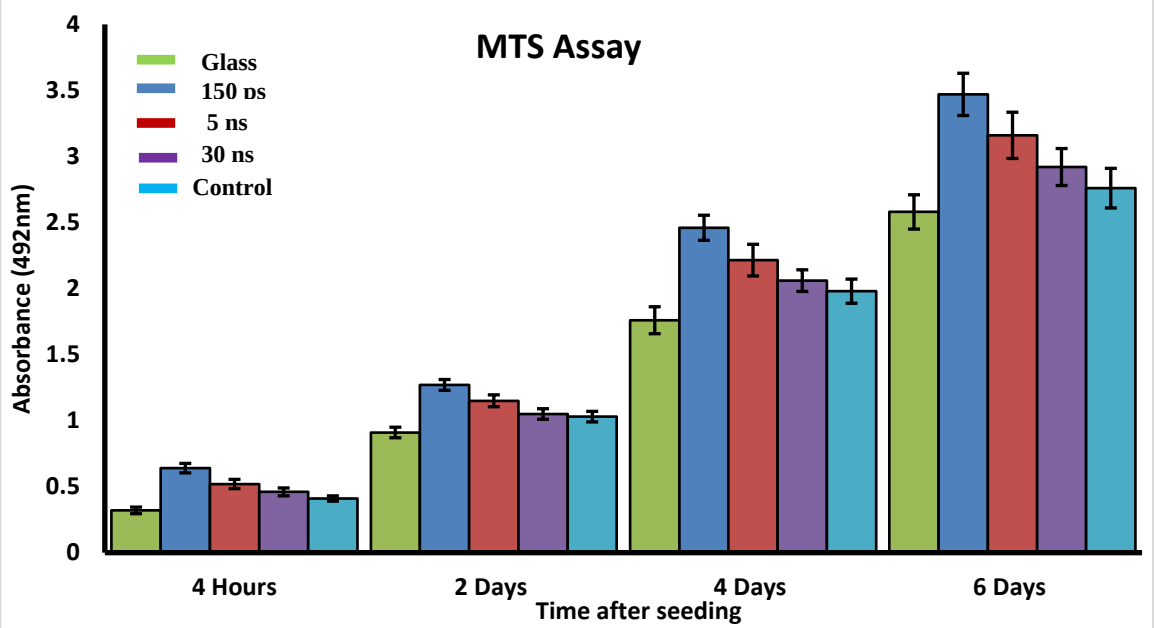

Figure 5.9: MTS result of samples produced with different laser pulse duration before and after immersion in SBF.

Fluorescent microscope images of cells attached on the surface of samples produced with different laser frequencies

Cell adhesion properties of TiO2 coatings were determined by the F-actin staining assay of the samples with BMSC (Figure 5.10(a)). The primary adhesion of 4 hours after cell seeding is shown in Figure 5.10 (b), where the hBMSC cultures on glass sample show a

round shape, and almost no spreading presents on the surface. In contrast, the complete spreading of hBMSC cultures on the S1 sample is observed.

The trend of the metabolic activity of BMSC on the samples was similar to 4 hours, which could be due to the results of primary cell attachment, not the toxicity of the surface. The adhesion and proliferation of BMSC on NFTi coated glass significantly increased when laser pulse duration decreased, indicating that the NFTi prepared by the shortest laser pulse duration (150 ps) receives more suitable substrate for cell culture. Moreover the F-actin filament immunofluorescent staining shows the higher cell spreading and cell attachments of S1 compared to the uncoated sample. The higher cell adhesion to the TiO2 coated surface is due to topography, roughness, porosity, wettability, surface energy, and protein adsorption/absorption. These data illustrated the higher biocompatibility interaction between cell and the coated surface, even in comparison with the standard surface of cell culture (TCP).

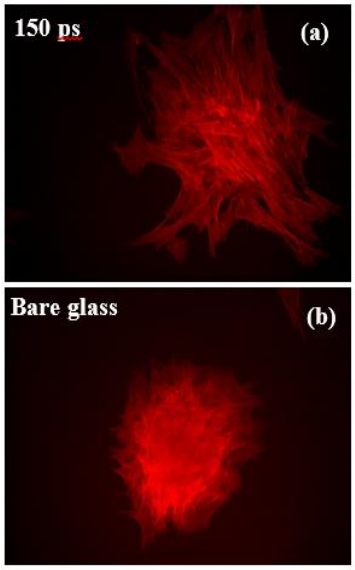

Figure 5.10: Fluorescent microscope images of cell attached on the surface of (a) sample produced with 150 ps lase pulse duration, (b) bare glass.

5.1.Summary

Samples prepared with constant laser power, constant laser frequency and changeable laser pulse duration	Samples prepared with laser power = 9 W, frequency = 1200 KHz, pulse duration = 150 ps	Samples prepared with laser power = 9 W, frequency = 1200 KHz, pulse duration = 5 ns	Samples prepared with laser power = 9 W, frequency = 1200 KHz, pulse duration = 30 ps
NFTi amount	High	Less	Least
Biocompatibility	High	Less	Least

6. Chapter Six

6.1. Result summary

Our research work was done in three different procedures. The conclusions we arrived at were that the HILIRT laser procedure was a superior method of surface modification without changing bulk properties or the chemical properties of the surface.

In the first results chapter we focused on changing the laser power without changing the other parameters, and the results showed that by changing laser power, the amount of titanium nanofibres increased; also the SVR of the nanofibres increased, which generates more HA-like laser production and more biocompatibility of the samples after immersing them in SBF. The more biocompatibility we have, the more viable the sample is, and the less toxicity we have. To put it briefly, the more nanofibres we have, the more cell adhesion on samples we have, and the more compatible implants we have for use in biomedical end tissue engineering.

In the second results chapter we focused on the laser frequency parameter and did not change the others. The results for this parameter are similar to the laser power results. In other words, by increasing laser frequency we have more generation of titanium nanofibres, and more suitable places for cell adhesion elements to nucleate and grow on. It means that by increasing laser frequency we have better biocompatibility, better MTT results, which shows the vitality percentage of the cell, and better cell adhesion.

In the third result chapter we came through the most tests possible, and was the most important part of this research. In this chapter we changed laser pulse duration without changing laser power, frequency or other parameters. The results for increasing laser pulse

duration were opposite to the results for increasing laser power and frequency. By increasing laser pulse duration, the amount of titanium nanofibres decreased, and the shape of fibres changed to agglomerated particles. These results show that by increasing laser pulse duration, the samples' biocompatibility, which is the ability to produce HA-like layers after immersion in SBF, decreased, because there were fewer suitable places for cell adhesion agent elements to nucleate and grow on the specimens. Consequently, by increasing laser pulse duration, the toxicity of samples increased after contacting with cells and the number of healthy cells on the specimens increased,

These results all show that when using HILIRT method for the surface modification of implants, the laser pulse duration should not be high, and in contrast the laser power and frequency amount should be as high as possible.

6.2. Future Work

The work done in this study suggests many ideas for future research. For instance, the HILIRT method can be done exactly on bioactive glass, which is more and more biocompatible with body and took researchers attention.

Also, as we know that implants and scaffolds in body have specific lifespans, obtaining corrosion results can help us understand the length of their stay in the body without hazardous problems.

In this research we used only titanium sheets to produce titanium nanofibres which are really biocompatible with body; we can also use other kinds of materials to increase this biocompatibility and to add other properties such as antibacterial properties to implants.

Producing a specific pattern on implants to trigger cells for attachment is a novel idea for biomedical applications, because it creates more suitable patterns for specific body tissues such as nerve tissues to be generated and healed better.

In this research the titanium nanofibres were just deposited on the glass, without any adhesion materials; however we can evaluate some biocompatible body glue to increase adhesion of nanofibres on samples and obtain better endurance.

Additionally, the procedure of NFTi formation can be simulated and modelled by a good theoretical model to predict other laser parameters effects on nanofiber generation and cell behaviors.

As everyone knows, all biomedical research related to human should always be done first on animals and afterwards on humans, so we can have in-vivo tests additionally to the in vitro test on the lab-on-the-chip.

References

1. Chen, F.M. and Liu, X., 2016. Advancing biomaterials of human origin for tissue engineering. Progress in polymer science, 53, pp.86-168.

2. Williams, D.F. ed., 1987. Definitions in biomaterials: proceedings of a consensus conference of the European Society for Biomaterials, Chester, England, March 3-5, 1986(Vol. 4). Elsevier Science Limited.

3. Kokubo, T., Kushitani, H., Sakka, S., Kitsugi, T. and Yamamuro, T., 1990. Solutions able to reproduce in vivo surface-structure changes in bioactive glass-ceramic A-W3. Journal of Biomedical Materials Research Part A, 24(6), pp.721-734.

4. Kokubo, T. and Takadama, H., 2006. How useful is SBF in predicting in vivo bone bioactivity?. Biomaterials, 27(15), pp.2907-2915.

5. Hench, L. L., & Andersson, O. (1993). Bioactive glass coatings. Advanced Series in Ceramics, 1, 239-260.

6. Ouis, M. A., Abdelghany, A. M., & ElBatal, H. A. (2012). Corrosion mechanism and bioactivity of borate glasses analogue to Hench's bioglass. Processing and Application of Ceramics, 6(3), 141-149.

7. Jones, M.H. and Jones, S.H., 2003. Wet-chemical etching and cleaning of silicon. Fredericksburg, Va.: Virginia Semiconductor.

8. Buckberry, L. and Bayliss, S., 1999. Porous silicon as a biomaterial. Materials World, 7(4), pp.213-215.

9. Dhanekar, S. and Jain, S., 2013. Porous silicon biosensor: current status. Biosensors and bioelectronics, 41, pp.54-64.

10. Colpitts, C., & Kiani, A. (2018). Laser processing of silicon for synthesis of better biomaterials. *Biomaterials in Regenerative Medicine*, *4*, 229.

11. Amorphous silicon-SiO2 textures. Journal of applied biomaterials & functional materials, 15(1), pp.84-92.

12. Qiu, Z.Y., Chen, C., Wang, X.M. and Lee, I.S., 2014. Advances in the surface modification techniques of bone-related implants for last 10 years. Regenerative biomaterials, 1(1), pp.67-79.

13. Kiani, A., Venkatakrishnan, K. and Tan, B., 2009. Micro/nano scale amorphization of silicon by femtosecond laser irradiation. Optics express, 17(19), pp.16518-16526.

14. M. S. Brown and C. B. Arnold, "Fundamentals of laser-material interaction and application to multiscale surface modification," in Laser precision microfabrication: Springer, 2010, pp. 91-120.

15. Hermawan, H., Biodegradable metals: from concept to applications. 2012.

16. Safaie, N., Jones-Taggart, H., & Kiani, A. (2019). High Intensity Laser Induced Reverse Transfer: Solution for Enhancement of Biocompatibility of Transparent Biomaterials. Coatings, 9(9), 586.

17. Elias, C. N., Lima, J. H. C., Valiev, R., & Meyers, M. A. (2008). Biomedical applications of titanium and its alloys. *Jom*, *60*(3), 46-49.

18. Gepreel, M. A. H., & Niinomi, M. (2013). Biocompatibility of Ti-alloys for long-term implantation. *Journal of the mechanical behavior of biomedical materials*, *20*, 407-415.

19. Safaie, N., & Kiani, A. (2018). Enhancement of bioactivity of glass by deposition of nanofibrous Ti using high intensity laser induced reverse transfer method. *Vacuum*, *157*, 92-99.

20. Beigi, M. H., Safaie, N., Nasr-Esfahani, M. H., & Kiani, A. (2019). 3D Titania Nanofiber-Like Webs Induced by Plasma Ionization: A New Direction for Bioreactivity and Osteoinductivity Enhancement of Biomaterials. *Scientific Reports*, *9*(1), 1-17.

21. Hamza, S., Ignaszak, A. and Kiani, A., 2017. Synthesis of electrical conductive silica nanofiber/gold nanoparticle composite by laser pulses and sputtering technique. Nanoscale research letters, 12(1), p.432.

22. Williams, D. F. (1999). The Williams dictionary of biomaterials. Liverpool University Press.

23. Park, J., & Lakes, R. S. (2007). Biomaterials: an introduction. Springer Science & Business Media.

24. Vroman, I., & Tighzert, L. (2009). Biodegradable polymers. *Materials*, *2*(2), 307-344.

25. Hermawan, H. (2012). Biodegradable metals: from concept to applications. Springer Science & Business Media.

26. Daniel, I. M., Ishai, O., Daniel, I. M., & Daniel, I. (1994). *Engineering mechanics of composite materials* (Vol. 3, pp. 256-256). New York: Oxford university press.

27. Sames, W. J., List, F. A., Pannala, S., Dehoff, R. R., & Babu, S. S. (2016). The metallurgy and processing science of metal additive manufacturing. *International Materials Reviews*, *61*(5), 315-360.

28. Standard, A. S. T. M. (2006). F67, 2006. Standard Specification for Unalloyed Titanium, for Surgical Implant Applications (UNS R50250, UNS R50400, UNS R50550, UNS R50700), ASTM International, West Conshohocken, PA.

29. Standard, A. S. T. M. (2008). F136–08e1 Standard Specification for Wrought Titanium-6 Aluminum-4 Vanadium ELI (Extra Low Interstitial) Alloy for Surgical Implant Applications (UNS R56401). *West Conshohocken, PA: ASTM International*.

30. Standard, A. S. T. M. (2005). F2063-05. Standard specification for wrought nickel-titanium shape memory alloys for medical devices and surgical implants. West Conshohocken, PA: ASTM International.

31. ASTM, F. (2005). F2063: Standard Specification for Wrought Nickel-Titanium Shape Memory Alloys for Medical Devices and Surgical Implants. *West Conshohocken: ASTM International*.

32. Vallet-Regí, M. (2001). Ceramics for medical applications. *Journal of the Chemical Society, Dalton Transactions*, (2), 97-108.

33. Kokubo, T. (Ed.). (2008). Bioceramics and their clinical applications. Elsevier.

34. Marti, A. (2000). Inert bioceramics (Al2O3, ZrO2) for medical application. *Injury*, *31*, D33-D36.

35. Dehestani, M., Zemlyanov, D., Adolfsson, E., & Stanciu, L. A. (2017). Improving bioactivity of inert bioceramics by a novel Mg-incorporated solution treatment. *Applied Surface Science*, *425*, 564-575.

36. Graves Jr, G. A., & Kumar, B. (1986). *U.S. Patent No. 4,604,097*. Washington, DC: U.S. Patent and Trademark Office.

37. Törmälä, P., Välimaa, T., Niiranen, H., Pohjonen, T., & Rokkanen, P. (2002). *U.S. Patent No. 6,406,498*. Washington, DC: U.S. Patent and Trademark Office.

38. Bagha, P. S., Khakbiz, M., Safaie, N., Sheibani, S., & Ebrahimi-Barough, S. (2018). Effect of high energy ball milling on the properties of biodegradable nanostructured Fe-35 wt.% Mn alloy. *Journal of Alloys and Compounds*, *768*, 166-175.

39. Jung, D. R., Kapur, R., Adams, T., Giuliano, K. A., Mrksich, M., Craighead, H. G., & Taylor, D. L. (2001). Topographical and physicochemical modification of material surface to enable patterning of living cells. *Critical reviews in biotechnology*, *21*(2), 111-154.

40. Navarro, M., Michiardi, A., Castano, O., & Planell, J. A. (2008). Biomaterials in orthopaedics. *Journal of the royal society interface*, *5*(27), 1137-1158.

41. Dhanekar, S., & Jain, S. (2013). Porous silicon biosensor: Current status. *Biosensors and bioelectronics*, *41*, 54-64.

42. Colpitts, C., Ektesabi, A. M., Wyatt, R. A., Crawford, B. D., & Kiani, A. (2016). JABFM.

43. Jones, M. H., & Jones, S. H. (2003). Wet-chemical etching and cleaning of silicon. *Fredericksburg, Va.: Virginia Semiconductor*.

44. Qiu, Z. Y., Chen, C., Wang, X. M., & Lee, I. S. (2014). Advances in the surface modification techniques of bone-related implants for last 10 years. *Regenerative biomaterials*, *1*(1), 67-79.

45. Hildebrand, H. F., Blanchemain, N., Mayer, G., Chai, F., Lefebvre, M., & Boschin, F. (2006). Surface coatings for biological activation and functionalization of medical devices. *Surface and Coatings Technology*, *200*(22-23), 6318-6324.

46. Kiani, A., Venkatakrishnan, K., & Tan, B. (2009). Micro/nano scale amorphization of silicon by femtosecond laser irradiation. *Optics express*, *17*(19), 16518-16526.

47. Kiani, A., Venkatakrishnan, K., Tan, B., & Venkataramanan, V. (2011). Maskless lithography using silicon oxide etch-stop layer induced by megahertz repetition femtosecond laser pulses. *Optics express*, *19*(11), 10834-10842.

48. Reif, J. (2010). Basic physics of femtosecond laser ablation. In *Laser-Surface Interactions for New Materials Production* (pp. 19-41). Springer, Berlin, Heidelberg.

49. Kiani, A., Patel, N. B., Tan, B., & Venkatakrishnan, K. (2015). Leaf-like nanotips synthesized on femtosecond laser-irradiated dielectric material. *Journal of Applied Physics*, *117*(7), 074306.

50. Tan, B., & Venkatakrishnan, K. (2009). Synthesis of fibrous nanoparticle aggregates by femtosecond laser ablation in air. *Optics express*, *17*(2), 1064-1069.

51. Shaheen, M. E., Gagnon, J. E., & Fryer, B. J. (2014). Femtosecond laser ablation behavior of gold, crystalline silicon, and fused silica: a comparative study. *Laser Physics*, *24*(10), 106102.

52. Radmanesh, M., & Kiani, A. (2016). Bioactivity enhancement of titanium induced by Nd: Yag laser pulses. *Journal of applied biomaterials & functional materials*, *14*(1), 70-77.

53. Williams, D. F. (2008). On the mechanisms of biocompatibility. *Biomaterials*, *29*(20), 2941-2953.

54. Anderson, J. M., & Miller, K. M. (1984). Biomaterial biocompatibility and the macrophage. *Biomaterials*, *5*(1), 5-10.

55. Adewumi, O., Aflatoonian, B., Ahrlund-Richter, L., Amit, M., Andrews, P. W., Beighton, G., ... & Blum, B. (2007). Characterization of human embryonic stem cell lines by the International Stem Cell Initiative. *Nature biotechnology*, *25*(7), 803.

56. Arora, M. (2013). Cell culture media: a review. *Mater Methods*, *3*(175), 24.

57. Braydich-Stolle, L., Hussain, S., Schlager, J. J., & Hofmann, M. C. (2005). In vitro cytotoxicity of nanoparticles in mammalian germline stem cells. *Toxicological sciences*, *88*(2), 412-419.

58. Patro, N. M., Sultana, A., Terao, K., Nakata, D., Jo, A., Urano, A., ... & Rohit, S. (2014). Comparison and correlation of in vitro, in vivo and in silico evaluations of alpha, beta and gamma cyclodextrin complexes of curcumin. *Journal of Inclusion Phenomena and Macrocyclic Chemistry*, *78*(1-4), 471-483.

59. Hendow, S. T., & Shakir, S. A. (2010). Structuring materials with nanosecond laser pulses. *Optics express*, *18*(10), 10188-10199.

60. Paladiya, C., & Kiani, A. (2019). Synthesis of Silicon Nano-fibrous (SiNf) thin film with controlled thickness and electrical resistivity. *Results in Physics*, *12*, 1319-1328.

7. Appendix

https://www.sciencedirect.com/science/article/abs/pii/S0042207X18310741

Vacuum 157 (2018) 92–99

Contents lists available at ScienceDirect

Vacuum

journal homepage: www.elsevier.com/locate/vacuum

Enhancement of bioactivity of glass by deposition of nanofibrous Ti using high intensity laser induced reverse transfer method

Naghmeh Safaie, Amirkianoosh Kiani*

Silicon Hall: Micro/Nano Manufacturing Facility, Faculty of Engineering and Applied Science, University of Ontario Institute of Technology (UOIT), Ontario, Canada

ABSTRACT

The aim of this research is to develop a new method for the enhancement of bioactivity of glass and transparent materials by the deposition of Ti nanofibrous structures generated by a high intensity laser induced reverse transfer method (HILIRT). Titanium nanofibers with different porosity, fiber diameter, and bioactivity are synthesized at various ranges of pulse frequency, power, and scanning speed combined with the HILIRT method. Features and bioactivity of these deposited Ti coatings before and after seven days immersion in simulated body fluid are compared. The results show increasing laser frequency and laser power leads to more Ti nanofiber generation and enhanced biocompatibility, while increasing laser scanning speed results in lower Ti nanofiber growth and lower biocompatibility. Combination of the laser parameters such as frequency, power, and scanning speed can optimize the deposited Ti nanofiber properties for a wide range of biomedical applications using transparent biomaterials such as implanted optoelectronics and light guiding devices, lab on a chip (LoC) and in-vitro and real time analysis of living cells in laboratories.

1. Introduction

These days, with developments in tissue engineering, biomaterials are designed to be in contact with the body's organs [1]. Biomaterials are utilized in medical devices and interact with the biological system [2]. Since they are used in connection with living tissues, they have to be biocompatible [1]. Transparent biomaterials (e.g. bioactive glass) are used extensively in biomedical applications due to their optical properties and quality of tissue regeneration [3]. Bioactive glass, sometimes called bioglass, has the ability to form a hydroxyapatite (HA)-like surface layer when it interacts with bone cells or is soaked in simulated body fluid (SBF) [4]. The ability to make an HA-like layer in biomaterials is a desirable property since it increases the bioactivity of materials, resulting in better interaction with surrounding living tissue and lower risk of rejection [5]. Although bioactive glass is one of the silicate-based glasses that has lower SiO_2 content and higher CaO/P_2O_5 ratio compared to durable silicate glass [3], surface modification should be conducted to minimize toxicity and the possibility of failure. Some common methods to modify the surface of biomaterials are chemical etching, photolithography, and mechanical processing [6–11]. However, all these methods suffer from disadvantages including chemical process (toxic materials and not environmentally friendly), multi-step, time consuming and expensive fabrication process. The laser induced reverse transfer (LIRT) method is a novel laser processing technique that can be used to modify the surfaces of transparent materials such as glass and reduce failure of the treated material after implanting in the body through optimizing the material's surface properties such as absorption, chemistry, roughness, and bioactivity [12]. Using LIRT for deposition of nano-particles and nano fibers of gold, silicon and hybrid materials have been reported previously [13–16]; however, none of the proposed methods has been used for deposition of biocompatible materials and evaluated by in-vitro tests for potential use in biomaterials engineering. LIRT can be employed to deposit the biocompatible metallic elements on the material's surface to increase the generation of the HA-like layer and eventually increase cell conductivity and adhesion [17]. There are some metallic elements, which are used in biomedical applications, especially in implant generations, such as Mg, Fe, Ti, and others [18,19]. Each of these elements has its own properties, such as biodegradation, strength, and biocompatibility. Amongst them Mg, Fe, and their alloys are used in biodegradable implants [18], while Ti is the most biocompatible metallic element used in implant generation and scaffolds in the past [20]. Ti also can be alloyed with other biocompatible elements such as Fe, Mn, Sn, and Si in medical and dental applications, as these possess high mechanical properties without metal retrogression [21]. These Ti alloys are favored as implants in hard tissue engineering such as artificial knee and hip joints, screws for fixation, bone plates, pacemakers, and artificial hearts [20]. In dental applications, Ti can be used for bridges, crowns, screws, abutments, and as dental restoration wiring when alloyed with Ni and its own shape-memory effect [18]. Although Ti-6Al-4V is widely used in Ti alloys for biomedical applications due to its resistance to pitting and corrosion and its great tensile strength [14], there is a move to replace

* Corresponding author.
E-mail address: amirkianoosh.kiani@uoit.ca (A. Kiani).

https://doi.org/10.1016/j.vacuum.2018.08.035
Received 26 June 2018; Received in revised form 25 July 2018; Accepted 18 August 2018
Available online 21 August 2018
0042-207X/

https://www.mdpi.com/2079-6412/9/9/586

coatings

MDPI

Article

High Intensity Laser Induced Reverse Transfer: Solution for Enhancement of Biocompatibility of Transparent Biomaterials

Naghmeh Safaie [1], Holly Jones-Taggart [2] and Amirkianoosh Kiani [1,*]

[1] Silicon Hall: Micro/Nano Manufacturing Facility, Faculty of Engineering and Applied Science, Ontario Tech University, Oshawa, ON L1GOC5, Canada; Naghmeh.Safaie@uoit.ca
[2] Faculty of Health Sciences, Ontario Tech University, Oshawa, ON L1GOC5, Canada; Holly.JonesTaggart@uoit.ca
* Correspondence: amirkianoosh.kiani@uoit.ca

Received: 30 August 2019; Accepted: 16 September 2019; Published: 17 September 2019

check for updates

Abstract: Bioactive glass is used extensively in biomedical applications due to its quality and effectiveness in tissue regeneration. Bioactive glasses are able to interact with biological systems and can be used in humans to improve tissue regeneration without any side effects. Bioactive glass is a category of glasses that maintain good contact with body organs and remain biocompatible for a long time after implementation. They have the potential to form a hydroxyapatite surface as a biocompatible layer after immersion in body fluid. In this research, glass biocompatibility was modified using a deposition method called the high intensity laser induced reverse transfer (HILIRT) method and they were utilized as enhanced-biocompatibility bioactive glass (EBBG) with a correspondent nanofibrous titanium (NFTi) coating. HILIRT is a simple ultrafast laser method for improving implants for biomedical applications and provides a good thin film of NFTi on the glass substrate that is compatible with human tissue. The proposed method is a non-chemical method in which NFTi samples with different porosities and biocompatibilities are synthesized at various laser parameters such as power and frequency. Physical properties and cell compatibility and adhesion of these NFTi before and after immersion in simulated body fluid (SBF) were compared. The results indicate that increasing laser intensity and frequency leads to more NFTi fabrication on the glass with no toxicity and better cell interaction and adhesion.

Keywords: laser nanofabrication; nano fibrous biomaterials; biocompatibility; transparent materials

1. Introduction

Transparent materials such as glass have extensive applications in biomedical science, and since they react with physiological fluids and form tenacious bonds to hard and soft tissues through cellular activity, they have to be compatible with biologic organs and surrounding living tissues [1–5]. Surface modification is one of the methods of changing surface properties such as roughness, absorption, chemistry and the general structure of materials to enhance the biocompatibility without altering material bulk properties [6–9]. Methods used to modify surface properties include chemical, physical and chemophysical treatments like electrochemical etching or photolithography, and these are costly and toxic [6–10]. Another modification process reported previously is to apply an enhanced thin layer on the substrate with a laser without changing the bulk properties [8,11,12]. The primary objective of this research is to compare different parameters of introduced ultrashort pulsed laser processing to enhance the biocompatibility of glass for biomedical use. In this study, nanofibrous titanium (NFTi) on glass substrate was prepared by the high intensity laser induced reverse transfer

https://www.nature.com/articles/s41598-019-54533-z

SCIENTIFIC REPORTS
natureresearch

OPEN

3D Titania Nanofiber-Like Webs Induced by Plasma Ionization: A New Direction for Bioreactivity and Osteoinductivity Enhancement of Biomaterials

Mohammad-Hossein Baigi[1,2], Naghmeh Safaie[1], Mohammad-Hossein Nasr-Esfahani[2] & Amirkianoosh Kiani[1*]

In this study, we describe the formation method of web-like three-dimensional (3-D) titania nanofibrous structures coated on transparent substrate via a high intensity laser induced reverse transfer (HILIRT) process. First, we demonstrate the mechanism of ablation and deposition of Ti on the glass substrates using multiple picosecond laser pulses at ambient air in an explicit analytical form and compare the theoretical results with the experimental results of generated nanofibers. We then examine the performance of the developed glass samples coated by titania nanofibrous structures at varied laser pulse durations by electron microscopy and characterization methods. We follow this by exploring the response of human bone-derived mesenchymal stem cells (BMSCs) with the specimens, using a wide range of *in-vitro* analyses including MTS assay (colorimetric method for assessing cell metabolic activity), immunocytochemistry, mineralization, ion release examination, gene expression analysis, and protein adsorption and absorption analysis. Our results from the quantitative and qualitative analyses show a significant biocompatibility improvement in the laser treated samples compared to untreated substrates. By decreasing the pulse duration, more titania nanofibers with denser structures can be generated during the HILIRT technique. The findings also suggest that the density of nanostructures and concentration of coated nanofibers play critical roles in the bioreactivity properties of the treated samples, which results in early osteogenic differentiation of BMSCs.

Although, bone autograft and allograft are considered the gold standard for bone regeneration, the associated risk of donor site morbidity and limited supplements remain disadvantages of these methods. Tissue engineering approaches, as a promising alternative, aim to facilitate bone regeneration, even in large craniofacial skeletal defects[1–4].

Among different tissue engineering methodologies, bone tissue engineering with the support of stem cells is of great interest considering their ability to differentiate into a variety of cells and their self-renewal ability[5]. Human mesenchymal stem cell (hMSCs) differentiation is an ethical way of tissue remodeling. Simply, cell and Extracellular Matrix (ECM) interaction is mutual: cells affect and are affected by ECM[6,7]. Indeed, the physical properties of surfaces that ECM forms, such as structure, topography, and physical and chemical properties, influence MSC livability and self-restoration, differentiation, and proliferation[8]. MSCs, which dwell in the bone marrow and other tissues, are able to regenerate damaged tissues when employed in specific scaffolds and implanted into defect sites[9]. Cultured-cell to ECM and their adjacent cell interaction plays a crucial role in cell viability and adhesion, proliferation, migration, and differentiation, as well as bone remodeling and osseointegration. These two factors (materials and cells) will be completed by a preferable fabrication method as the third side of the bone tissue engineering, which can provide a desirable platform for these to work together. Several methods are currently used to produce bone tissue engineering surfaces including sol-gel (20), hydrothermal 10[6],

[1]Silicon Hall: Micro/Nano Manufacturing Facility, Faculty of Engineering and Applied Science, Ontario Tech University, Ontario, Canada. [2]Department of Cellular Biotechnology Cell Science Research Center, Royan Institute for Biotechnology, ACECR, Isfahan, Iran. *email: amirkianoosh.kiani@ontariotechu.net